



**UNIVERSIDAD DE INVESTIGACIÓN DE  
TECNOLOGÍA EXPERIMENTAL YACHAY**

**Escuela de Ciencias de la Tierra, Energía y Ambiente**

**TÍTULO: VOLCANIC EVENT CHARACTERIZATION USING  
SEISMIC SIGNALS: AN EXAMPLE FROM LASCAR  
VOLCANO, CHILE.**

Trabajo de integración curricular presentado como requisito para  
la obtención de título de Geólogo

**Autor:**

Monar Lucero Jhuliana Geraldinne

**Tutor:**

MSc. Pérez Roa Richard

**Co-tutor:**

PhD. Foster Anna Elizabeth

Urququí, julio 2023

## AUTORÍA

Yo, **JHULIANA GERALDINNE MONAR LUCERO**, con cédula de identidad 0202683090, declaro que las ideas, juicios, valoraciones, interpretaciones, consultas bibliográficas, definiciones y conceptualizaciones expuestas en el presente trabajo; así como, los procedimientos y herramientas utilizadas en la investigación, son de absoluta responsabilidad de la autora del trabajo de integración curricular. Así mismo, me acojo a los reglamentos internos de la Universidad de Investigación de Tecnología Experimental Yachay.

Urcuquí, julio 2023.

---

Jhuliana Geraldinne Monar Lucero  
CI: 0202683090

## AUTORIZACIÓN DE PUBLICACIÓN

Yo, **JHULIANA GERALDINNE MONAR LUCERO**, con cédula de identidad 0202683090, cedo a la Universidad de Investigación de Tecnología Experimental Yachay, los derechos de publicación de la presente obra, sin que deba haber un reconocimiento económico por este concepto. Declaro además que el texto del presente trabajo de titulación no podrá ser cedido a ninguna empresa editorial para su publicación u otros fines, sin contar previamente con la autorización escrita de la Universidad.

Asimismo, autorizo a la Universidad que realice la digitalización y publicación de este trabajo de integración curricular en el repositorio virtual, de conformidad a lo dispuesto en el Art. 144 de la Ley Orgánica de Educación Superior

Urcuquí, julio 2023.

---

Jhuliana Geraldinne Monar Lucero

CI: 0202683090

## DEDICATION

*To my beloved family, for their unwavering support throughout this journey and every step of my life. Each milestone I have reached is a testament of their boundless motivation and uplifting spirit. In times of adversity, they have been, and will forever be, my steadfast pillar, providing strength and solace.*

Jhuliana Geraldinne Monar Lucero

## ACKNOWLEDGMENTS

I would like to express my heartfelt gratitude to my family for their limitless support, constant encouragement, and infinite patience. Their unconditional love and unwavering trust have been a constant source of inspiration throughout this entire journey.

I also want to extend my deepest appreciation to all the professors at Yachay Experimental Technology Research University for their dedicated efforts in sharing their knowledge. A special thank you goes to my thesis co-supervisor, PhD. Anna Foster, whose years of teaching not only served as a source of inspiration but also for her dedication to this research endeavor. Her valuable comments, insightful suggestions, and expert guidance were instrumental in the success of my project and my overall academic growth. I would also like to express my gratitude to PhD. Rafael Almeida for his motivating words and the immense trust he has placed in me.

To all my friends, I am profoundly grateful. You have been the reason why every moment of my university life has been filled with joy. Thank you for your constructive criticism, valuable advice, and unwavering support. Your presence has been a crucial factor in completing this marvelous phase of my life. I want to express a special appreciation to my long-standing friends: Mikaela, Paola, and Sahori. And to my friends who have taught me that time holds no significance when we connect on a spiritual level, my beloved pointlovers: Patricio, Jaime, Laila, Kristina, and Roberth.

Lastly, I would like to express my heartfelt gratitude to each and every person who offered me their academic and personal support. To all the professors who have been a part of my university journey, you hold a special place in my heart, and your influence will forever remain with me.

Jhuliana Geraldinne Monar Lucero

## **Resumen**

Volcanes presentan un sistema complejo que puede ser estudiado utilizando diversos métodos geológicos. Entre estos métodos, las señales sísmicas juegan un papel crucial en la comprensión de los procesos internos del volcán, así como en la estructura y dinámica de los cuerpos magmáticos y sistemas de plomería. La caracterización adecuada de estas señales es esencial para identificar diferentes tipos de eventos y su ubicación, e inferir su mecanismo fuente. El patrón temporal de estos eventos también puede proporcionar información valiosa para predecir futuros episodios volcánicos. Sin embargo, la tarea de localizar con precisión los eventos sísmicos puede ser desafiante debido a factores como la composición del magma y la topografía del volcán, así como al número limitado de estaciones de monitoreo disponibles.

Para abordar este problema, probaremos dos métodos para identificar eventos sísmicos utilizando datos de Lascar, un estratovolcán ubicado en el norte de Chile. La red 8E instalada alrededor de las laderas del volcán durante 2014-2015 nos proporcionó datos de forma de onda de seis estaciones de banda ancha, que utilizaremos para identificar eventos utilizando el método STA/LTA. Luego, calcularemos nueve parámetros basados en Kettner & Power (2013) para clasificarlos en diferentes tipos de eventos. Luego aplicaremos un método de búsqueda en cuadrícula desarrollado por Gottschämmer & Surono (2000) para localizar eventos de alta frecuencia y compararemos nuestros resultados con los de Gaete et al. (2019). Nuestro resultado incluye un catálogo de eventos de alta resolución, su clasificación en tipos LP, VT, Híbridos y Explosivos, y las ubicaciones de los eventos de alta frecuencia. Además, proporcionamos todo el código Python escrito para este estudio, tanto para reproducibilidad como para su aplicación futura en otros conjuntos de datos.

La información obtenida de este estudio proporcionará una comprensión más profunda de la dinámica del volcán Lascar, que también se puede aplicar a otros volcanes para reducir el riesgo de disturbios volcánicos para las ciudades cercanas.

**Palabras clave:** estaciones de monitoreo, eventos sísmicos, catálogo de eventos.

## **Abstract**

Volcanoes present a complex system that can be studied using various geological methods. Among these methods, seismic signals play a crucial role in understanding the internal processes of the volcano, as well as the structure and dynamics of magmatic bodies and plumbing systems. Proper characterization of these signals is essential to identify different types of events and their location, and to infer their source mechanism. The temporal pattern of these events can also provide valuable information to predict future volcanic episodes. However, the task of accurately locating seismic events can be challenging due to factors such as the composition of the magma and the topography of the volcano, as well as the limited number of available monitoring stations.

To address this issue, we will test two methods identify seismic events, using data from Lascar, a stratovolcano located in northern Chile. The 8E network installed around the volcano's flanks during 2014-2015 provided us with waveform data from six broad-band stations, which we will use to identify events using the STA/LTA method, we then calculate nine parameters based on Kettner & Power (2013) to classify them into different event types. We will then apply a grid search method by Gottschämmer & Surono (2000) to locate high-frequency events and compare our results with those of Gaete et al. (2019). Our outcome includes a high-resolution catalog of events, their classification into LP, VT, Hybrid, and Explosive types, and the locations of high-frequency events. Additionally we provide all the python code written for this study for both reproducibility and future application to other data sets.

The information obtained from this study will provide a deeper understanding of the dynamics of Lascar volcano, which can also be applied to other volcanoes to reduce the risk of volcanic unrest for nearby cities.

**Key words:** monitoring network, seismic events, event catalog.

# INDEX

1	INTRODUCTION.....	1
1.1	Seismology.....	2
1.1.1	Volcano seismology.....	2
1.2	Seismic Monitoring System.....	3
1.2.1	Seismic Network and Instruments.....	3
1.3	Importance of Volcano Monitoring and Forecasting.....	4
1.4	Seismic Signals.....	5
1.4.1	Transient seismic signals.....	5
1.4.2	Continuous seismic signals.....	6
1.4.3	Temporal, amplitude, and frequency properties.....	7
1.5	Noise in the data.....	9
1.6	Objectives.....	10
2	GEOLOGICAL SETTING.....	10
2.1	Tectonic Setting.....	11
2.2	Geology.....	13
2.2.1	Stratigraphic Succession.....	14
2.3	Eruptive History.....	17
3	METHODOLOGY.....	18
3.1	Data.....	19
3.2	Downsampling and filtering.....	20
3.3	Identification of Seismic Events.....	21
3.4	Seismic Event Properties.....	22
3.4.1	Temporal Metrics.....	22
3.4.2	Amplitude Metrics.....	23
3.4.3	Spectral Metrics.....	24
3.5	Events Classification.....	26



3.5.1	Type of volcanic event .....	26
3.5.2	Manual Classification .....	26
3.5.3	Automated Classification .....	27
3.6	Noise Awareness.....	28
3.7	Swarm Detection.....	28
3.8	VT Events Location .....	28
3.8.1	Grid Method .....	29
3.9	Application.....	30
4	RESULTS .....	31
4.1	Data.....	31
4.2	Filtering and Downsampling .....	32
4.3	Identification of Seismic Events .....	33
4.4	Seismic Event Properties .....	34
4.4.1	Metrics calculation Python code .....	35
4.4.2	Identified Events.....	41
4.5	Events Classification.....	41
4.5.1	Manual Classification .....	41
4.5.2	Automated Classification .....	46
4.5.3	Identified and Classified Events .....	48
4.6	Noise Awareness.....	48
4.7	Filtered Events .....	50
4.8	Event Location .....	53
5	DISCUSSION .....	57
5.1	Temporal, amplitude and spectral metrics.....	57
5.2	Comparison with published study.....	58
5.3	Multistation vs Single Station Detection .....	59
5.4	Benefits and Limitations .....	60

5.5	Interpretations of Events .....	60
6	CONCLUSIONS.....	62
6.1	Recommendations and Future Work .....	63
7	References .....	64
	ANNEXES .....	74
	ANNEX 1: Events Recognition.....	74
	ANNEX 2: Single Station Detection noise removal for stations BB1, BB2, BB3, BB4, and BB5. ....	79
	ANNEX 3: Final events after noise removal .....	81
	ANNEX 4: Events Location .....	82
	ANNEX 5: Example for one high frequency event location .....	87

## LIST OF FIGURES

- Figure 1.** Location map of Lascar volcano (blue triangle) with respect to the Northern Volcanic Zone (NVZ), Central Volcanic Zone (CVZ), Southern Volcanic Zone (SVZ), and Austral Volcanic Zone (AVZ). The red triangles shows the distribution of volcanoes in South America. *Source:* USGS Tectonic Plates base map (Scheibner et al., 2013), satellite basemap by Esri, and UC Berkley Geodata Repository for volcanic distribution (Smithsonian Institution et al., 2003) ..... 12
- Figure 2.** Geological framework of Lascar volcano (Coordinate System: WGS84 – UTM zone 19S). a) Digital Elevation Model of Lascar: geomorphological features of western and eastern stratocones and five nested craters. b) Simplified Geological Units and Evolutionary Stages of Lascar Volcano. *Source:* The geological information, vents location, and faults descriptions were taken from Bertin et al., (2022). ..... 15
- Figure 3.** Methodology flowchart for volcano-seismic signal analysis..... 18
- Figure 4.** Lascar volcano elevation map using UTM Zone 19S coordinate system. Location of the temporary network: BAS, BB1, BB2, BB3, BB4, and BB5. *Source:* the digital elevation model was taken from Bertin et al., (2022). ..... 19
- Figure 5.** Data obtained from GFZ Data Centre for LascarVolcano during 2014-2015 31
- Figure 6.** Seismic signal recorded in Lascar Volcano April 9th, 2014. a) BB3 station seismogram with a sample rate of 200 Hz without filtering. b) Seismogram of processed data (downsampling/decimation) with a sample rate of 100 Hz. The data was filtered with a high-pass filter of 13600 Hz and low-pass filter of 40 Hz..... 32
- Figure 7.** The STA/LTA ratio is displayed graphically as follows: a) Seismogram from April 9, 2014 of Lascar volcano, with the red dashed line indicating the moment the STA/LTA ratio crosses the upper threshold, and the blue dashed line marking the lower threshold. b) The STA/LTA values for the April 9th, 2014 seismogram are shown. c) A close-up view of one anomaly identified by the STA/LTA method between 21:06:40 and 21:08:20 on April 9, 2014. .... 33
- Figure 8.** Frequency bands determination for visual classification. 15 events were separated into 3 frequency-based clusters: red for low frequency, black for high frequency, and blue for mixed frequency signals..... 42
- Figure 9.** Manual classification example for low frequency events. This event occurred in March 4, 2015 recorded at BB4 station. a) Normalized spectral amplitude over

frequency. The description of the event like FI, RMSa, Ton, and Toff are described in the upper right corner. b) Amplitude over time. The amplitude data for the event are presented in blue. The red line represents the beginning of the events and blue dashed line the end of the event. ....43

**Figure 10.** Manual classification example for high frequency event. This signal was recorded on March 4, 2015 at BB4 station. a) Normalized spectral amplitude over frequency domain. b) Amplitude over time for the event occurred from 03:16:31 to 03:16:40. ....44

**Figure 11.** Manual classification example for hybrid events. The exemplified event was recorded at Lascar on March 4, 2015. a) Normalized spectral amplitude over frequency with a maximum NSA at lower frequencies. b) Amplitude over time of an event occurred at 07:09:54 and end at 07:10:06. ....45

**Figure 12.** K-means cluster analysis for RMS amplitude values of the calibration set. The center of each cluster is denoted by an X, and the gray dashed lines represent the thresholds. The low frequency events are represented by black dots, while the hybrid frequency and high frequency events are denoted by red and blue dots, respectively. ....47

**Figure 13.** During 2014-2015, events were identified at Lascar volcano, including 75,509 high frequency events, 32,687 low frequency events, 17,749 hybrid events, and 1,083 explosion events. ....48

**Figure 14.** Volcano-Tectonic signal recorded at Lascar Volcano in station 8E.BB3 on August 11, 2014 at 04:50. This event was filtered using a band-pass filter between 0.2 to 10 Hz. a) Spectrogram for VT event, where lowest values are represented by blue and highest by white. b) Seismogram for VT event recorded in HHZ channel. ....50

**Figure 15.** Hybrid signal identified at Lascar on August 11, 2014 at 04:48 in the morning. This events was filtered between 1 and 10 Hz. a) Spectrogram for HYB event with a minimum frequency varying from 0.2 to approximately 5 Hz at the beginning of the signal, then reaching a frequency of 10 Hz. b) Seismogram of HYB event recorded in HHZ channel. ....51

**Figure 16.** Low-frequency signal recorded at Lascar Volcano on December 3, 2014 at 22:51. The LP event was filtered using a band-pass filter between 0.2 and 10 Hz. a) Spectrogram for LP event with a minimum frequency varying from 0.2 to approximately 5 Hz. b) Seismogram of LP event recorded in HHZ channel. ....52

<b>Figure 17.</b> Very Long Frequency event recorded at Lascar volcano on BB5 station on June 30, 2014. a) Spectrogram for a VLF event, the frequency content ranges from 0.2 to 4 Hz. b) Seismogram for VLP occurred from 21:54:05 to 21:54:09.....	53
<b>Figure 18.</b> Velocity estimation for the location of four different high-frequency events. The best velocity, producing the minimum standard deviation, is listed for each event. ....	54
<b>Figure 19.</b> Location estimation for high frequency events recorded at Lascar volcano during 2014-2015. a) High frequency events recorded from January 2014 to May 2015 (green circles). b) High frequency events recorded in 2015 (yellow circles). c) High frequency located events in 2014 (red circles). ....	56
<b>Figure 20.</b> A comparison of volcano-tectonic earthquake (VT) locations. b) VT event locations found in our study (blue dots), and VT events found by Gaete et al. (2019; orange dots). c) locations of VTs (in green) from our study and the VTs (red circles) and long-period (LP) events (blue circles) published by Gaete et al. (2019).....	59
<b>Figure 21.</b> Daily average of Long-Period events and LP/VT ratio calculated from April 2014 to May 2015.....	61
<b>Figure 22.</b> Event rate maximum value for each day in the period 1 January 2014 - 25 May 2015.....	62

## LIST OF TABLES

<b>Table 1.</b> Description of the stations available in Lascar volcano during 2014-2015.....	20
<b>Table 2.</b> Statistical description for the FI threshold calculation .....	47
<b>Table 3.</b> SSD Noise thresholds determination for BAS station .....	49
<b>Table 4.</b> Description of selected events for velocity estimation. Arrival time ( $T_{arr}$ ) values are in seconds and $V_{guess}$ values are in km/s.....	55

# 1 INTRODUCTION

Volcanic eruptions are events that occur daily worldwide and on several occasions have caused the loss of many lives (e.g. 25000 deaths in Nevado del Ruiz, 30000 in Mt. Pelé, 36000 in Krakatau, and 90000 in Tambora). The consequences of these events can be reduced by studying earthquakes, ground motion, remote satellite analysis, volcanic gases, rock and water chemistry, besides the use of specialized instruments (seismometer, tiltmeter, thermal imaging, InSAR, infrasound, geochemical analysis, etc.). For this project, the main observation will be earthquakes using the seismic signals that come from the volcano. The branch of geosciences that allows us to analyze these signals, which describe how waves travel on earth, is seismology. Seismology is an effective tool when we try to forecast volcanic eruptions (McNutt, 1996). To obtain the greatest amount of seismic information from a volcano, it is important to have a fixed monitoring system that records the volcano's internal movements daily. The greater the number of stations, the better the records, and also the forecasts. With constant seismic monitoring, we can recognize seismic signatures and patterns that are directly associated with eruptive activity (Sassa, 1935 & Falsaperla et al., 2020). Throughout history, there have been successful forecast cases of volcanic eruptions that have reduced damage and losses through an early warning. One of the clearest examples is the eruption of Mount Pinatubo (June 15, 1991) in which around 60,000 people were evacuated, thus preventing the possible death of thousands and the loss of hundreds of millions of dollars (Harlow et al., 1996).

Lascar volcano is one of the most active and hazardous stratovolcanoes in the Central Andes of Chile (Figure 1). Its activity is characterized by a history of explosive eruptions and persistent fumarolic activity (Gaete, 2020). Despite its remote location, Lascar presents a significant hazard to nearby populated areas due to its potential for explosive eruptions that can generate pyroclastic flows, lahars, and ash fall. Seismic monitoring is a crucial tool for characterizing the activity of Lascar volcano and assessing its potential for hazardous eruptions (McNutt, 2000). Seismic signals can provide insights into the internal processes of the volcano, such as the movement of magma and fluids, and can help identify different types of events, such as volcanic tremors, long-period earthquakes, and high-frequency earthquakes. The classification of these events is essential for understanding the behavior of

the volcano and predicting future volcanic episodes. For instance, long-period earthquakes can indicate the presence of a pressurized magma reservoir (Chouet et al., 2003), whereas high-frequency earthquakes can suggest the fracturing of rocks due to volcanic deformation (Wauthier, C., Roman, D.C., & Poland, M.P., 2013; Yukutake, Y., et al., 2021; Song, Z., Tan, Y.J., & Roman, D.C., 2023). Therefore, an accurate classification of seismic events can provide valuable information for hazard assessment and risk mitigation.

## **1.1 Seismology.**

During an earthquake, energy is released and transmitted throughout Earth; and radiated as seismic waves. Seismology is the science that describes those waves and analyzes the information we can get from those signals. Depending on the observations and instrumentation, the degree of uncertainty in the seismic studies change is why it is essential to collect data as much as possible; thus, we can develop a realistic model of the interior of the Earth at any scale.

In seismology, the waves are classified into two main types: body waves which radiate through solid material, and surface waves which travel along free surfaces (Shearer, 2009). Within body waves, there are **P-waves** (compressional waves) and **S-waves** (shear waves). The P-waves travel horizontally, changing the volume and shape. Since P-waves arrive first, those signals are vital when estimating the location of the event. The S-waves propagate without changing the volume of the material. The most exciting characteristic of S-waves is that the signal does not transmit through molten material ("Body waves inside the earth", 2021).

### ***1.1.1 Volcano seismology.***

Volcano seismology is a subfield of seismology specialized in the study of seismic signals that come from volcanoes and are related to volcanic activity (Zobin, 2012). It is important to differentiate the volcanic earthquakes and tectonic earthquakes since the terminology and even the interpretations tend to contrast with each other. Seismicity at volcanos differs from common tectonic earthquake sources since it describes the movement of the ground for specific conditions closely related to the volcano structure (Wassermann, 2012). The seismic signals coming from a volcano differ in their continuity and frequency, forming swarms, compared to strong and long-lasting signals in common earthquakes (McNutt, 2005;



Wassermann, 2012). The high-frequency events in both volcano and tectonic earthquakes are mostly caused by slip on faults. The only way to differentiate them is with the pattern of occurrence. The low-frequency events are usually interpreted to be the result of fluid-pressurization in the interior of the volcano (McLaskey, Thomas, Glaser, & Nadeau, 2012; McNutt, 2005). Volcano seismology allows the development of new analysis techniques focused on the physical properties of the volcanic edifice such as topography, wave velocity or attenuation, which indicate variations in the total composition of the material (McNutt, 2005).

## **1.2 Seismic Monitoring System.**

Seismic monitoring allows us to identify any change in the current status of the volcano seismicity (McNutt, 2000). There are many instruments and techniques that we can use to infer the activity inside the volcano. Monitoring volcanic activity should include several methods and observations like earthquakes, ground motion, remote satellite analysis, volcanic gases, and rock and water chemistry (USGS, n.d). The seismic study has become the main reliable source of information about the volcano. In volcanic environments, the increase of seismic activity is often related to volcanic unrest (Brill, Waite, & Chigna, 2018; McNutt, 2000; Tilling, 2008).

The main goal of seismic monitoring is precisely located seismic events (Zobin, 2012), and to relate the type of event to a physical process (McNutt, 2000). According to McNutt (2000), seismic monitoring can give us the information to determine if a volcano is restful, restless, shows precursory activity, in eruption, or is restful after the activity. The seismic monitoring provides us the data required to identify any anomalous signal. Ideally, the data should represent a continuous observation at regular intervals from normal to active status (Council, 1994). This is important to establish the normal and the unusual signals, which can vary from volcano to volcano.

### ***1.2.1 Seismic Network and Instruments.***

A seismic station is composed of recorders and sensors, while a seismic network is a set of stations that collect and join the data for subsequent analysis (Havskov & Alguacil, 2015). The seismic network can be permanent or temporary. Some of the instruments used in a seismic station are seismometer, gravimeter, GPS, and correlation spectrometer (COSPEC).

The seismometer is an instrument based on the principle of inertia, where a magnetic mass is suspended on a spring; the data is generated when the mass moves (e.g., McNutt, 2000). Then, the seismograph records the motion of the ground. The data that is obtained by the seismograph is called a seismogram. Those provide us the parameters to evaluate the origin of the earthquake, magnitudes, and locations (Council, 2006). In recent times, three-component digital broadband seismometers are the most used since the seismic waves can be analyzed in three dimensions and at different frequencies.

### **1.3 Importance of Volcano Monitoring and Forecasting.**

Activity monitoring can give us an early warning of an imminent eruption and a guide to managing volcano-related hazards. As mentioned earlier, volcanic activity is generally accompanied by seismic anomalies. By analyzing the data obtained by the seismic network, in some cases forecasts can be made with great accuracy. This will depend on the quality of the data. Not only the observations and the instrumental measurements at the volcano are used to deduce the dynamics of the active volcano but also to reduce the volcanic risk (tilling, 2008). The historical behavior of the volcano plays a crucial role since it allows us to establish a baseline for anomalous behavior. With this information the preparation of hazard assessments is feasible.

There are clear examples of successful volcano seismic monitoring, one of them is the volcanic eruption at Mount St. Helens in October 2004 reviewed and discussed in Driedger et al., (2004). There was recorded a 2-day swarm and shallow volcano-tectonic events on 23 September, this behavior was compared with the historical records of Mount St. Helens seismicity and cataloged as a precipitation-related anomaly. On September 25, the magnitude of the earthquakes increased from less than 1 to 2.8 increasing the chance of hazardous activity (Zobin, 2012). By September 26, the U.S. Geological Survey-Cascade Volcano Observatory (USGS-CVO) and Pacific Northwest Seismic Network (PNSN) had issued the corresponding alert of volcanic unrest and possible eruption. In the subsequent days with increasing activity, land and air roads were closed.

On the other hand, according to the report presented by Global Volcanism Program (1985), the eruption of Nevado del Ruiz in November 1985 was one of the biggest death tolls ever registered with more than 25000 deaths. The volcanic activity started in September and

increased in November with volcanic tremors and high-frequency seismic swarms. By 13 November, an explosive eruption melted the ice generating massive lahars which covered the town of Armero. The lack of volcanic monitoring and hazard assessments contributed to the elevated death tolls.

#### **1.4 Seismic Signals**

The observations of volcanic earthquakes had left evidence of seismic signals purely related to volcanic activity. The seismic signals associated with tectonic and volcanic earthquakes are slightly different. The first description and classification of volcano seismic signals was made by Shimozuru (1972) and Minakami (1974) and was based on the appearance of the seismograms. According to Wassermann (2012), the seismic signals can be grouped into transient and continuous signals.

##### ***1.4.1 Transient seismic signals***

Bormann & Wielandt (2013) in their study point out that most of the seismic signals are transient waveforms that spread out radially in a medium from a localized seismic source. This type of signal is mainly used to locate the origin and then relate these event locations to the physical processes of the medium. The following description of the volcano signals is based on the work of McNutt (1996, 2000), Wassermann (2012), and Zobin (2012).

***Deep Volcano-Tectonic events (A-type)*** occur below about 2 km depth with well-distinguished P- and S- wave arrivals, high frequency, and short signal duration. A-type signals appear before and during the eruption. These events are associated with shear failure along the fault plane, the same mechanism of tectonic earthquakes. The main characteristic of A-type (VT-A) and that differentiates it from an ordinary tectonic earthquake is that this type of event occurs in swarms without a defined mainshock.

***Shallow Volcano-Tectonic events (B-type)*** occur above 2 km near the crater with clear P-wave onsets and often indistinguishable S-wave arrivals, low frequency, and high scattering. B-type events occur in swarms by the shear failure caused by a double-couple source.

*Volcano-tectonic earthquakes* are related to the migration of the magma towards the surface. The magma escapes through fluid-filled cracks like dikes or sills. The stress at the dike tip is denoted with  $\sigma_1$ , the principal stress  $\sigma_1$  is parallel to the dike. According to Rubin and Gillard

(1998), there are three cases that can explain VT earthquakes: fault slip away from the tip, fault slip near the tip and shear failure of surrounding rocks. On the other hand, Hill's (1977) model describes a cluster of fluid-filled cracks oriented parallel to the greatest principal stress  $\sigma_1$ . The shear failure occurs in the oblique fault planes that link the tips of the dikes (Zobin, 2003). Hill (1977) also suggests that the magnitude of the VT earthquakes is related to size of the magmatic intrusion and the spacing between dikes in the case of swarm. Both models are used to explain the source mechanism of VT earthquakes in intermediate and high viscosity magmas.

**Low-frequency events (LP)** are often related to shallow sources with a frequency that varies from 1 to 3 Hz. They do not show S-wave arrivals or clear onsets of P-waves. Long period-low frequency events are modeled as the result of resonating crack formations due to magma injection and changes in the pressure of the system.

**Hybrid events** are the result of a mixture of LP, A- and B-type likely due to combined source mechanisms. Long-period events can trigger volcano-tectonic events and vice versa. At the beginning of the seismogram the signal could look like a LP event but then the signal evolves to a characteristic VT signal.

**Explosion quakes** are very distinguishable signals since these are earthquakes often associated with explosive eruptions. Explosion quakes occur very frequently during eruptive phases, with several events per hour and short signal duration. These events present two significant phases, the first one of low-frequency followed by high-frequency signals (Ereditato & Luongo, 1997).

#### **1.4.2 Continuous seismic signals**

As was mentioned earlier, volcano-seismic events differ from tectonic seismicity due to the fact that signals of volcano-seismic events not only present transient phases but also long-lasting continuous phases. Continuous seismic signals are characterized by having a volcanic source.

**Volcanic tremors** can be deep or shallow, distinguished by the long signal duration ranging from minutes to hours with relatively constant amplitude (Zobin, 2012). McNutt et al., (1991, 1994) describe a general relationship between the maximum amplitude of volcanic tremors

and the volcanic explosivity index (VEI). Also, Tokarev et al., (1984b) show a correlation between the amplitude of the volcanic tremor to the height of the pyroclastic column during explosive eruptions; they also point out that hot material output coincided with the time of increasing volcanic tremors.

**Surface signals** are the result of surface processes like lahars, pyroclastic flows, debris flow, or rockfalls produced by an emergent dome or volcanic processes (Wassermann, 2012). This signal shows large amplitudes and high frequencies, above 5 Hz (Wassermann, 2012). Especially in volcanoes with glaciers, the study of surface signals is useful for hazard assessment.

#### ***1.4.3 Temporal, amplitude, and frequency properties***

Understanding the properties of volcano-related seismic events is crucial as it offers insight into the activity of a volcano and can aid in forecasting potential eruptions. The characteristics of seismic events, including amplitude, time, and frequency, can reveal information about the movement of magma and other geological processes occurring beneath the surface of a volcano.

The amplitude serves as an important tool for distinguishing real data from background noise and for identifying significant seismic events. It is worth noting that the maximum amplitude can be influenced by several factors, including the location and depth of the seismic source, the type of seismic waves generated, and the local geology and ground conditions (Mickus, K, 2021). As a result, the maximum amplitude should be considered in the context of other seismic parameters and observations when interpreting volcano-seismic signals. The Root-Mean-Square amplitude is a highly sensitive parameter that can detect small and large changes in amplitude, as noted in previous research (Sukmono, 1999; Pamungkas & Ridwana 2021). Since these waves have different velocities and amplitudes, the RMS amplitude is a useful tool for seismologists to compare the energy carried by different types of waves more accurately. The maximum amplitude, phase amplitude, and Root-Mean-Square (RMS) amplitude are commonly used amplitude metrics in volcano-seismic analysis.

The time in volcanic environments is a significant parameter to correlate between volcanic events and its source mechanism. The most prominent time-related parameters are: duration, events rate and the time between events. The duration of a volcanic earthquake is a parameter used to determine the type of volcanic activity that produced the earthquake. A longer duration can indicate a larger, more gradual release of energy (the relationship between energy and duration was first described by Bisztricsany, E. (1958)), which is typical of volcanic processes such as magma movement or deformation of the volcano (e.g., Seropian et al., 2021). A shorter duration can indicate a more explosive release of energy, which is typical of processes such as volcanic explosions or ash emissions (e.g. Hiroyuki et al., 2019; Schmid, Karstens & Nomikou, 2021). In general, longer-duration earthquakes are associated with more passive volcanic activity (volcanic tremor), while shorter-duration earthquakes are associated with more explosive activity (explosion quakes). A shorter gap between earthquakes suggests a higher activity rate, while a longer gap suggests a lower rate. These metrics can be used to estimate earthquake swarms, as they differentiate clusters of volcanic events based on the rate of activity (Godano et al., 2023).

The gap and event rate metrics are closely related, as both rely on the timing of event occurrences. In Pesicek et al. (2018) study, the authors emphasized the importance of considering multiple indicators in monitoring volcano and earthquake activity. This is because there have been instances where an eruption occurs without any corresponding change in the event rate. To provide a more complete picture of the state of a volcano and to make more accurate predictions about future activity, it is important to consider other indicators such as changes in ground deformation, gas emissions, and the temperature of hot springs near a volcano.

The spectral or frequency analysis is utilized in volcano-seismology to get valuable insights of the volcano dynamics. The maximum frequency can provide important information about the energy of high-frequency seismic waves. Higher frequencies typically correspond to shorter wavelengths, which are more attenuated as they propagate through the Earth's crust (Parmentier, E. M., 2015). Therefore, the maximum frequency can help in understanding the level of attenuation of seismic waves (Chen, 2020). The attenuation can be ruled by the geological context of the volcano, and therefore it may influence the seismic signal. Hence,

it is important to be mindful of the geological and structural characteristics of the studied volcano. The center frequency and the frequency index (FI) work together to define the lower- and upper-frequency bands (Buurman, & Wes, 2010), which vary between events. This makes it possible to establish a specific spectral analysis for each event. Even though this metric combination is a great strategy, there are some issues to address, such as the presence of noise. The FI is sensitive to frequency changes, and the noise might produce misinterpretations or wrongly classified events. Thus, the event classification accuracy depends on how good the noise removal is.

This information can be used by scientists to monitor and understand volcanic activity, make predictions about future eruptions, and inform decisions about evacuations and other safety measures. By studying the properties of volcano-related seismic events, scientists can gain a deeper understanding of how volcanoes work and improve their ability to predict and respond to volcanic eruptions.

### **1.5 Noise in the data**

The seismic signals that are not directly related to the volcanic process are classified as noise, so it is important to separate the useful data from seismic noise to avoid errors in the analysis and interpretation. Bormann & Wielandt (2013), describe several noise sources and the most relevant are five of them:

- Ambient vibrations due to natural sources like wind
- Man-made vibrations (transport, industry, etc.)
- Secondary signals (scattering).
- Effects of gravity
- Instrument-related noise.

To eliminate the noise it is necessary to know which the source is and also measure it. To avoid instrument-related noise it is necessary to calibrate according to the manufacturer's specifications, another seismometer can also be used to calibrate it (Bormann & Wielandt, 2013). Ambient noise and man-made vibrations can be deleted using Green's function and cross-correlations, besides this signal can also be used for volcano monitoring (Brenquier et al., 2011). The back-scattered noise is produced by the topography and shallow layers, so the

approach to extract the noise consist of two steps: modeling and then subtraction of the modeled noise events from the data (Montes, Vargas, & Pérez, 2005).

## **1.6 Objectives**

The main objectives of this study are to develop a methodology for identifying and characterizing volcanic events using seismic signals recorded at Lascar Volcano, Chile, and to provide insights into the seismicity and volcanic activity in the region. To achieve these objectives, our aim is to classify different types of seismic signals and volcanic events based on their properties and mechanism. Additionally, we plan to estimate the source location of volcanic events by employing seismic data inversion based on grid search method. Moreover, we will compare the results of our analysis with previous studies to assess the effectiveness of using seismic signals for characterizing volcanic events. By achieving these objectives, we aim to contribute to the development of seismic catalogs that contain comprehensive details about the volcanic activity. Furthermore, future studies based on our methodology can yield more accurate interpretations of volcanic events and their source mechanisms. Finally, by utilizing this catalog, we hope that future work will be able to develop effective volcanic hazard mitigation strategies based on the analysis of seismic signals.

## **2 GEOLOGICAL SETTING**

Lascar volcano, situated in the northern part of Chile at the east of the Atacama Desert (Figure 1), is a steep-sided stratovolcano composed of layers of volcanic ash, pumice, and hardened lava flows. Lascar volcano is located in the Andes mountain range, which is a result of the collision between the Nazca and South American tectonic plates. The volcano rises to a height of 5,592 meters above sea level (Figure 2), making it one of the tallest volcanoes in the Andes. Lascar volcano is part of a larger volcanic complex that includes several other volcanoes, such as Aguas Calientes, Olca, and Pili. It is widely acknowledged as one of the most active volcanoes within the Altiplano-Puna Volcanic Complex. The volcanic complex is thought to have formed over the last two million years (Quaternary), with the most recent eruption occurring in 2015. The Central Volcanic Zone, within which Lascar lies, is characterized by a crust that is exceptionally thick, ranging between 50 and 70 kilometers, as reported by Matthews et al. (1994).



The primary mode of volcanism in the region is andesitic-dacitic, resulting from complex processes such as fractional crystallization, magma mixing, and the assimilation of basaltic andesite injections, as reported by both Gaete et al. (2020) and Matthews et al. (1994). While the exact mechanisms driving the uprising of Lascar remain uncertain, geological evidence suggests that the volcano predates the last glacial maximum, according to Gardeweg et al. (1998).

## **2.1 Tectonic Setting**

The Andean mountain chain is a classic example of a convergent boundary where oceanic lithosphere is subducted beneath a continental margin. Specifically, the Nazca plate, which is an oceanic tectonic plate located to the west of South America, is subducting beneath the western margin of the South American plate. The subduction of the Nazca plate beneath the South American plate also results in the formation of a deep oceanic trench, known as the Peru-Chile Trench (Figure 1), which is located off the coast of South America. This trench is one of the deepest points in the Earth's crust, reaching a depth of over 8,065 meters (Lemenkova, 2019).

The volcanic activity in the Andes was divided into three main zones: Northern Volcanic Zone (NVZ), Central Volcanic Zone (CVZ), Southern Volcanic Zone (SVZ), and Austral Volcanic Zone (AVZ) (Figure 1). From latitude 14° to 28° S (Peru to Chile), the Central Volcanic Zone is considered one of the three major active volcanic zones along the Andes (De Silva, 1989) forming the western boundary of the Altiplano Plateau. The thickness of the crust beneath the CVZ is about 70 km from tectonic shortening, and the thickening is associated with subcontinental lithosphere thinning (Isacks, 1988; De Silva, 1989).

The CVZ has at least 50 active volcanoes. Most of the volcanoes in this region lie on a large Upper Tertiary ignimbrite plateau, one of the largest ignimbrite province in the world (De Silva, 1989). The Altiplano-Puna volcanic complex is a geological feature located in the Andes Mountains of South America, spanning across northern Chile, southwestern Bolivia, and northwestern Argentina. The Altiplano Plateau is an ignimbrite province resulting from

a Miocene ignimbrite flare-up, then called Altiplano-Puna volcanic complex, extending from latitude 21° to 24° (De Silva, 1989).

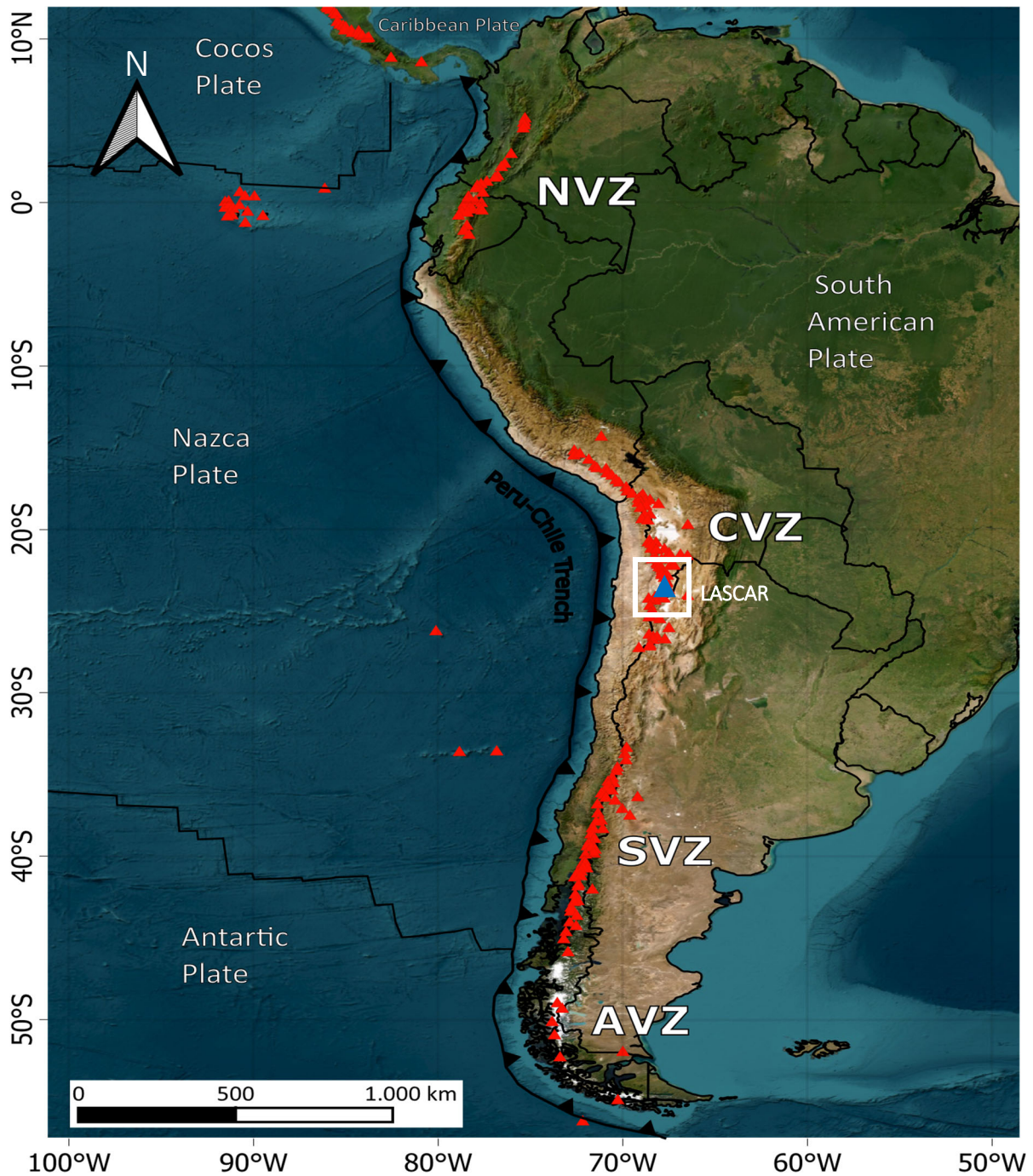


**Figure 1.** Location map of Lascar volcano (blue triangle) with respect to the Northern Volcanic Zone (NVZ), Central Volcanic Zone (CVZ), Southern Volcanic Zone (SVZ), and Austral Volcanic Zone (AVZ). The red triangles shows the distribution of volcanoes in South America. *Source:* USGS Tectonic Plates base map (Scheibner et al., 2013), satellite basemap by Esri, and UC Berkley Geodata Repository for volcanic distribution (Smithsonian Institution et al., 2003)

## 2.2 Geology

Lascar is a composite stratovolcano characterized by two superposed strato-cones and five nested craters of which the middle one is currently active (Figure 2a). Most of the Lascar activity is related to vulcanian eruptions with minor explosions due to hydrothermal infiltrations. The eruptive products are mainly andesites and dacites resulting from fractionation and mixing of mafic components and evolved magmas (Gardeweg, *et al.*, 2011; Matthew, 1994). The composition of the magma is produced by fractional crystallization (predominating plagioclase and pyroxene) and periodic magma mixing (Matthew, 1994). The difference between magmas is driven by shallow fractionation and continuous basaltic andesite injections (Matthew, 1994). The time between injections determines how basic or mafic the magma is.

In Lascar volcano there were identified at least 8 units that differ in age, lithology and depositional characteristics (Figure 2b). Based on the findings of Ramirez and Gardeweg (1982), the geological formation denoted as the unit Cerros de Salta/Cerros de Atama (**Lava Dome I**, Figure 2b) has been classified as a lava dome that originated during the Lower-Upper Pleistocene epoch. The age of this formation has been estimated to be between  $5.2 \pm 0.8$  to  $3.0 \pm 0.2$  million years, based on radiometric dating techniques (Ramirez & Gardeweg, 1982). Gardeweg (2011) characterized the **Lava Dome II** (Figure 2b), located in the Corona unit, as a lava dome that was formed during the Lower-Middle Pleistocene epoch. The estimated age of this formation ranges from  $1.36 \pm 0.14$  million years to  $540 \pm 30$  thousand years ago. According to the database compiled by Bertin et al. (2022), the Lascar region exhibits the presence of four distinct Pyroclastic Density Currents (PDCs): **PDC Deposits I** (Figure 2b), which correspond to the Tumisa formation, **PDC Deposits II** (Figure 2b) found in the Claile & Salta PFs unit, **PDC Deposits III** (Figure 2b) observed in the Aguas Calientes formation that dates back to the Lower-Middle Pleistocene epoch, and **PDC Deposits IV** (Figure 2b) located in the Soncor/Tumbre unit, dating back to the Upper Pleistocene-Holocene epoch. In contrast, Gardeweg (2011) and Brown (2021) have determined that **Mixed Volcanic Material I** (Figure 2b), found in the Lower-Middle Pleistocene Tumisa unit, has an age ranging from less than 2 million years to  $490 \pm 80$  thousand years. Additionally, Gardeweg (2011) has identified **Mixed Volcanic Material II** (Figure 2b), belonging to the Aguas Calientes formation from the same epoch as MVM I, with an

estimated age between  $430\pm 150$  to  $140\pm 15$  thousand years. However, Bertin et al. (2022) have reported the presence of a more recent lithographic structure called **Mixed Volcanic Material III** (Figure 2b), located in the Lascar unit and estimated to have formed during the Upper Pleistocene-Holocene period. Gardeweg (2011) reported the existence of a lava flow, referred to as **Lava Flow I** (Figure 2b), in the Lower-Middle Pleistocene period, with an estimated age range of  $240\pm 49$  to  $110\pm 40$  thousand years, located in the Lascar formation. Furthermore, Wörner (2000) and Gardeweg (2011) identified a younger lava flow stratum, named **Lava Flow II** (Figure 2b), situated in the Piedras Grandes unit, which dates back to the Upper Pleistocene-Holocene period, with an estimated age range of  $72\pm 10$  to  $7.17\pm 1.25$  thousand years. Finally, the **Pyroclastic Deposits** (Figure 2b) reported by Bertin et al. (2022) can be dated back to the Upper Pleistocene-Holocene period.

### **2.2.1 Stratigraphic Succession**

The stratigraphic succession of Lascar has been divided into four stages, each representing a specific geological period. From the oldest to the youngest: at the base of Lascar, we encounter the substratum (Permian-Triassic and Upper Cenozoic), followed by Lascar 1 (Pleistocene), Lascar 2 (Upper Pleistocene), Lascar 3 (Upper Pleistocene-Lower Holocene), and finally Lascar 4 (Holocene). These units have been differentiated based on their lithological characteristics, origin, and exposure, which describes the evolution of the volcanic complex and the changes in its morphology.

For our purpose the detailed description of the stratigraphic succession is not truly vital, but it is necessary to understand the characteristics of the volcano geology. Thus, for further information about the detailed stratigraphic characteristics like thickness, mineral composition and subunits petrology, we highly recommend Ramírez & Gardeweg, (1982); Matthews et al., (1994); Matthews et al., (1996); Matthews et al., (1997); Gardeweg et al., (1998); Matthews et al., (1999); Gardeweg *et al.* (2011); and Pérez (2020). The following description of the stratigraphic succession was taken from Gardeweg, *et al.* (2011) and Gardeweg et al. (1998):

**Substratum:** At the base of Lascar there are igneous and volcano-sedimentary rocks part of Permian-Triassic basement, and sediments and volcanic rocks from the Upper Cenozoic (Lila

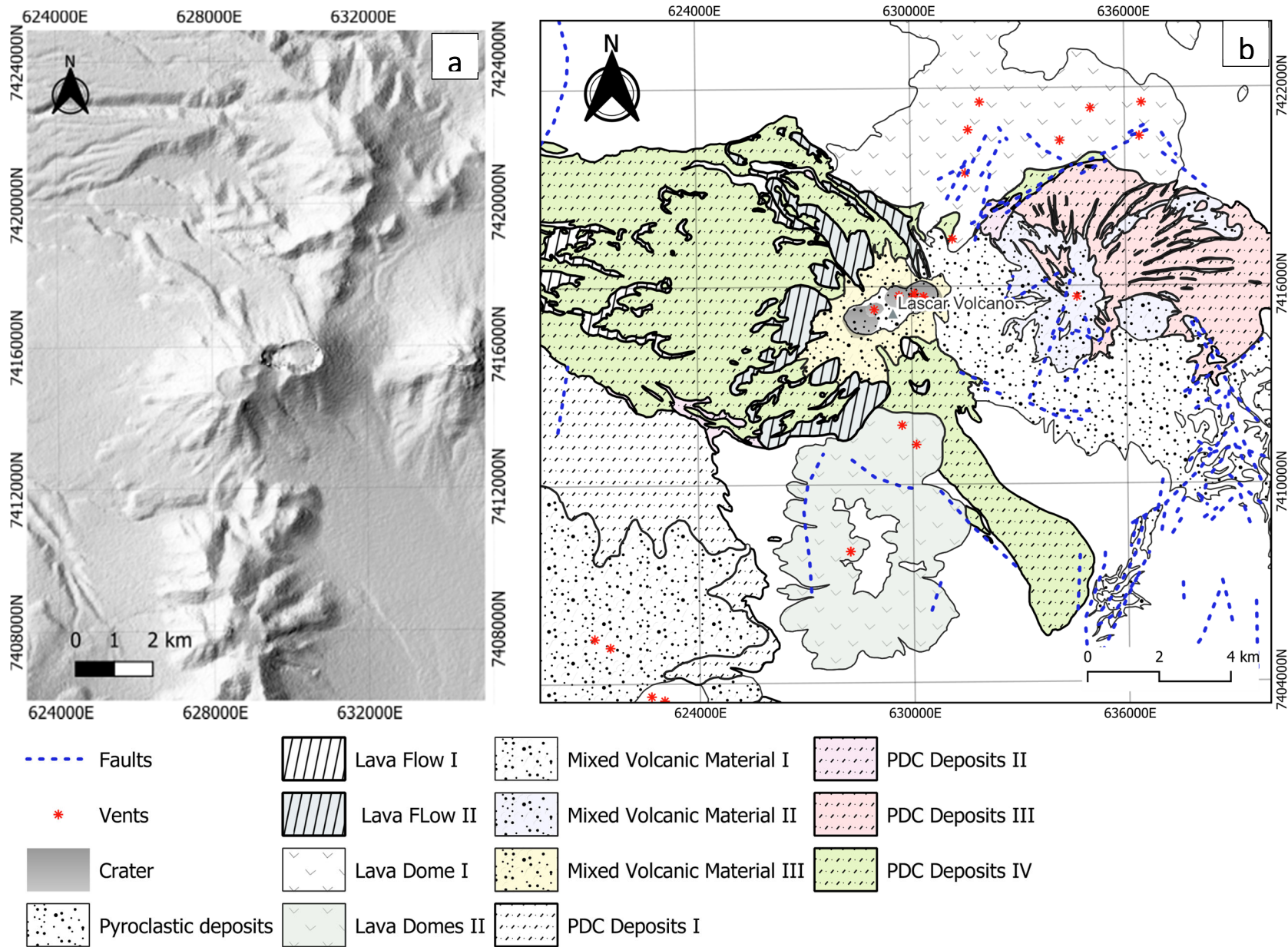


**Figure 2.** Geological framework of Lascar volcano (Coordinate System: WGS84 – UTM zone 19S). a) Digital Elevation Model of Lascar: geomorphological features of western and eastern stratocones and five nested craters. b) Simplified Geological Units and Evolutionary Stages of Lascar Volcano. Source: The geological information, vents location, and faults descriptions were taken from Bertin et al., (2022).

and Cas formations). The rocks of the basements occur as fault-bounded inliers being surrounded by recent volcanic rocks. Being part of substratum it was recognized five geological bodies: Peine group, Permian-Triassic granitoids, Quepe strata, Dacitic domes, and Ignimbrite Plateau.

**Láscar 1:** The initial stage of Lascar formation is characterized by the deposition of pyroclastic flow materials and the emplacement of extensive lava flows. The composition of lavas is mainly andesite lying over the Ignimbrite Plateau. This stage is composed by Stage I lavas (**Lava Flow I** and **Lava Dome I**, Figure 2b), Saltar and Chile units. Lascar 1 was developed at the eastern stratocone. It can be recognized by the coarse-grained andesitic pyroclastic flow deposits and mafic andesite lavas with the presence of pyroclastic agglutinates (**Mixed Volcanic Material I** and **PDC Deposits I**, Figure 2b).

**Láscar 2:** Migration stage, the volcanic vent migrates towards the west. The volcanic products represent a compositional change from andesite to more felsic andesite and dacites. Composed by pyroclastic flow deposits (**PDC II**, Figure 2b), lava flows (**Lava Flow II**, Figure 2b) forming the western cone. It is composed by Piedras Grandes deposits, Western stratocone lava flow, and Soncor ignimbrite. Lascar 2 is a major Plinian deposit and ignimbrite fan with a composition varying from rhyodacite to andesite, also, it was identified dacitic block-and-ash flow and glacier burst deposits. In this stage it was found indirect evidence that suggest a lava dome complex (**Lava Dome II**, Figure 2b)

**Láscar 3:** Low activity period and high erosion rate match with the regional humid climatic periods called Minchin. The humid climate helps the lahar formation changing the morphology of the volcanic deposits of Soncor. There is a period of reactivation with and explosion of pyroclastic flows mainly scoria (andesitic in composition) that will be related with the small pyroclastic cone nested into the large western crater and also the deposition of pyroclasts in the nearest zones. Besides, this event represents the ceasing of western cone activity and the subsequent migration to the eastern cone. This stage is characterized by pyroclastic flow deposits and Plinian deposits (**Mixed Volcanic Material III** and **PDC Deposits III**, Figure 2b)

**Láscar 4:** In Lascar 3 unit the eruptive events are west-oriented, after this stage the activity is re-directed to the east towards the Lascar 1 unit. Composed by andesitic lava flow,

vulcanian eruptions and subplinian eruption products (**PDC Deposits IV**, Figure 2b). At this stage were generated three nested craters in the western cone with a diameter varying between 600 and 1000 m. The craters formation is related to the collapse in the Lascar summit (Matthews *et al.*, 1997).

### **2.3 Eruptive History**

The eruptive history of Lascar is relatively young since the first record is estimated in 1848 with at least 30 eruptions (Petit-breuilh, 2004; Gardeweg *et al.*, 1994a; Philippi, R. A. & Petermann, A., 1856). Before 1986, the records of eruptive activity are quite vague since it is based on local stories or tales (Gardeweg, 1991). Casertano and Barozzi (1961) mention some eruptions in 1875, 1883, 1885, the end of 19<sup>th</sup> century, 1933, 1940, between November 1951 and January 1952, and 1959, but the records are irregular with inconsistencies. Most of the volcanic activity in Lascar is vulcanian and phreatic eruptions with ballistics (e.g. Gardeweg, 1991; Casertano and Barozzi, 1961). The volcanic products have significant presence of gas dominated by water steam (González-Ferrán *et al.*, 1995). From 1984 to 1996, Lascar activity was characterized by growth and subsidence of dacitic domes and occasional explosive episodes, where the subsidence is explained by the withdrawal of magma and decreasing permeability due to degassing at shallower parts of conduits (Matthew *et al.*, 1997). Subsequently, the impermeability of the system builds up as well as gas pressure, ending up in an explosive event. In 1993 there was an alteration in the cyclic activity since a more developed and gas-rich magma entered to the chamber provoking a Subplinian eruption. Afterward, the eruptive activity in Lascar has remained constant with passive degassing, minor explosive eruptions and few changes in the morphology of the active crater (Gardeweg *et al.*, 2011).

The latest notable eruptive event registered at Lascar volcano occurred in October, 2015. Historical records prior to this activity are scant and incomplete. Since 2013, the local authority responsible for monitoring volcanic activity in the area has been OVDAS (Observatorio Vulcanológico de los Andes del Sur), while the Servicio Nacional de Geología y Minería (SERNAGEOMIN) is the designated institution responsible for issuing changes in the alert level associated with Lascar volcano. According to the volcanic activity reports published by SERNAGEOMIN before October 30, 2015, there was an increase in seismic

activity, with a maximum magnitude of 2.5. In January 31, 2012, there was a swarm of 308 seismic events resulting in an ash column reaching a height of 0.5 km (Servicio Nacional de Geología y Minería [SERNAGEOMIN], 2012).

In April 2013, fumarolic activity accompanied by ash emissions and temperature anomalies at the crater were recorded, without any significant change in the seismic activity (SERNAGEOMIN, 2013a, 2013b). On July 26, 2013, screw-type seismic events (Long Period) associated with fluid dynamics at the conduit and precursory explosive events were recorded (SERNAGEOMIN, 2013c). Finally, on October 30, 2015, an ash column measuring 2500 meters in height and trending northeast from the volcanic edifice was detected, while the ground deformation was moderately low at 1 cm<sup>2</sup> (SERNAGEOMIN, 2015).

### 3 METHODOLOGY

This methodology aims to effectively identify, classify, and locate volcano-seismic signals (Figure 3). To achieve this, the dataset undergoes a series of preprocessing steps (described in Figure 3), including the utilization of bandpass filters and detrending techniques, to ensure a clean data set. Subsequently, the STA/LTA (Short-Term Average/Long-Term Average)

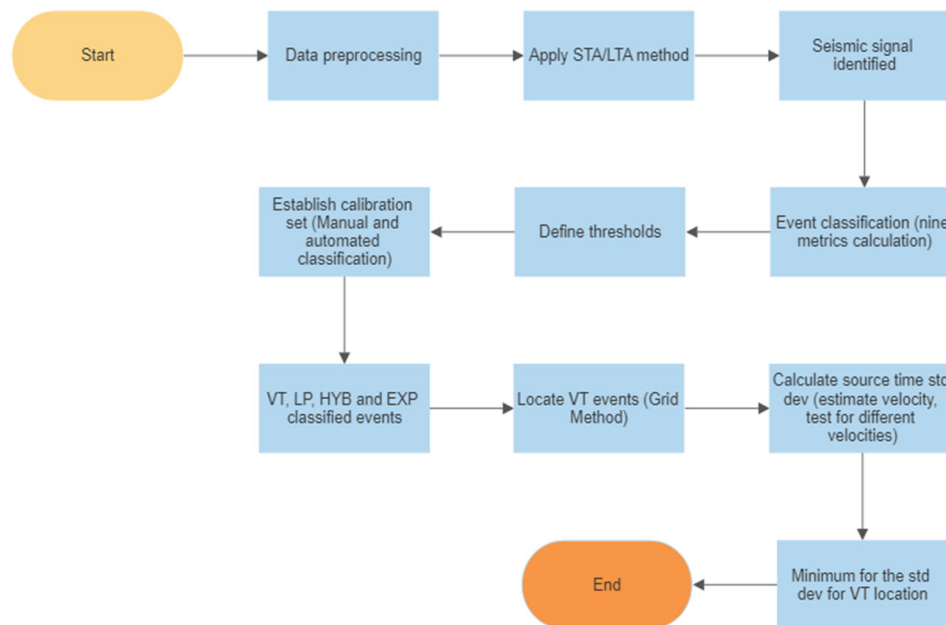


**Figure 3.** Methodology flowchart for volcano-seismic signal analysis.



ratio is calculated to identify seismic signals associated with volcanic processes. Upon event identification, nine distinct metrics are computed to characterize the identified events. These metrics play a crucial role in filtering out noisy events and facilitating the analysis of frequency content, ultimately enabling the classification of events into volcano-tectonic, long period, hybrid, and explosive signals. Additionally, the high-frequency events are localized using the grid method.

### 3.1 Data

The Lascar volcano was monitored for seismic activity from 2014 to 2015 using a temporary network (8E) installed by Walter et al. (2014) on its flanks (Figure 4). The network was set up in response to the 2014 Iquique earthquake in northern Chile to detect any changes in the volcano's state (Figure 4). It consisted of six broad-band stations, named BAS, BB1, BB2,

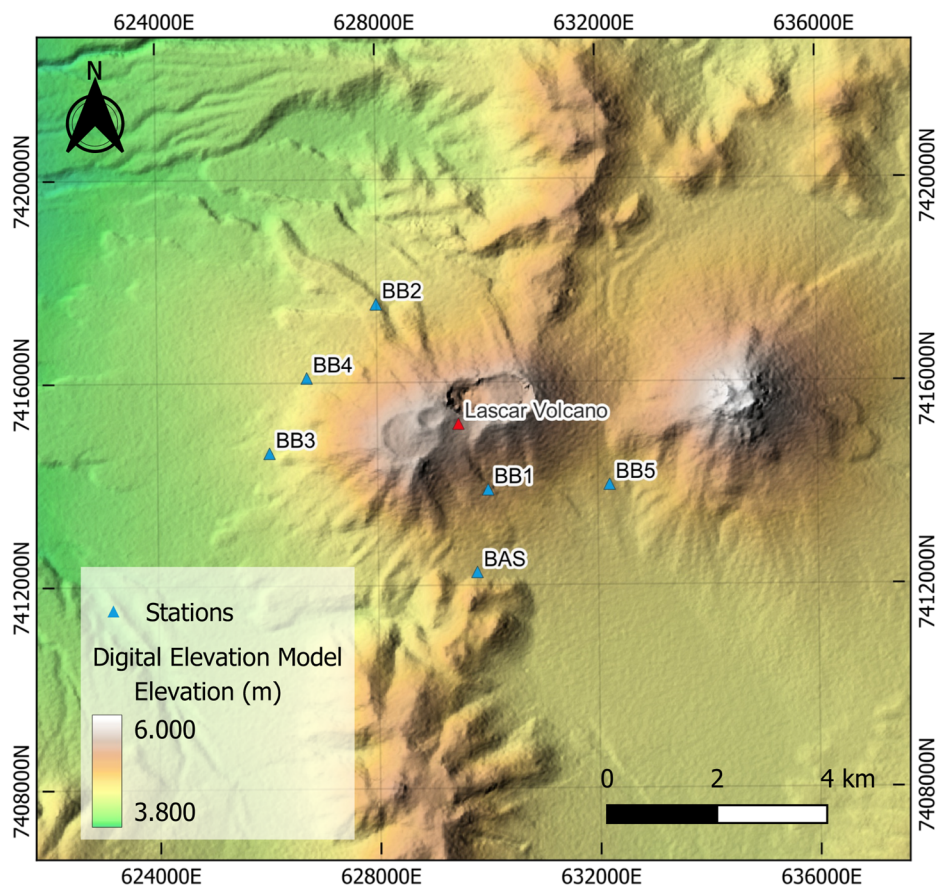


**Figure 4.** Lascar volcano elevation map using UTM Zone 19S coordinate system. Location of the temporary network: BAS, BB1, BB2, BB3, BB4, and BB5. Source: the digital elevation model was taken from Bertin et al., (2022).

BB3, BB4, and BB5 Hz (as listed in Table 1). These three-component seismic stations, installed by Walter et al (2014), were buried at a depth of 1 meter in the bedrock to reduce the influence of thermal variations and were powered by solar panels. All data collected by the seismometers was uploaded to the GFZ Helmholtz Centre Potsdam Data Service, which provides open access to both the waveform data and station metadata. For our purpose, the data were downloaded from the GEOFON data centre (GFZ) in MSEED format, which is a versatile file format that contains information about the station (metadata).

Unfortunately, the data for the BAS station only covers from January 01, 2014 to April 11, 2014, making it impossible to compare recordings between stations. As a result the BAS

**Table 1.** Description of the stations available in Lascar volcano during 2014-2015

Station	East*	North*	Altitude
BAS	629798.20	12258.90	4758.00
BB1	30006.70	13884.80	5026.00
BB2	627994.10	7417545.50	4668.00
BB3	626036.70	7414616.90	4422.00
BB4	626038	7414616.90	4604.00
BB5	632215.50	7413976.00	4785.00

\*UTM Zone 19s coordinate system

*Source: Walter et al., 2014*

station data cannot be used for event location, however, we can still use BAS station to classify events using Single Station Detection (SSD). Thus, it can still provide insight into the activity of Lascar volcano prior to more developed seismic activity. This study is based on data from April to August 2014 and from December 2014 to May 2015.

### 3.2 Downsampling and filtering

Most of the data has a sample rate of 100 Hz, but in the case of the BAS station, the data has a sample rate of 200 Hz. To maintain consistency in our analysis, we will reduce the sample rate from 200 Hz to 100 Hz through a process called 'downsampling'. This involves reducing

the number of samples or resolution of a signal, which will improve computation and data processing efficiency.

Also, we will apply bandpass filters to mitigate noise in the data set. Preprocessing is an important step in seismic signal analysis. Seismic data often contains a variety of noise sources and artifacts that can distort the underlying true signals (e.g. Allahverdiyeva, 2022 & Galluzzo et al., 2020). Even if this process will reduce the signals above and below the filter, it will still contains some noisy signals. To avoid that, we will use linear detrend, demean detrend, and cosine taper to carefully eliminate those signals (e.g, Williams, Perttu & Taisne, 2020). The linear detrend removed any linear trend or spurious signals caused by instrument drift (Williams, Perttu & Taisne, 2020). The demean trend technique the other hand involved removing the mean value of the data, as well as any biases or offsets in the data caused by variations in the sensor or instrument setup (Williams, Perttu & Taisne, 2020).

### 3.3 Identification of Seismic Events

The identification of seismic events requires the detection and picking of the P-phase arrival, as outlined by Li (2017). To calculate the time and location of the events, it is necessary to accurately define the P-phase arrival. While manual identification through visual examination of waveforms is possible, it is both time-consuming and subject to the examiner's judgment. With the high volume of data and the need for reliable results, an automatic method is necessary.

In order to automate the identification of the events, the Short-Term Average Long-Term Average (STA/LTA) method (Hafez et al., 2009, 2010) will be implemented. The STA/LTA ratios can be calculated by:

$$(k) = \frac{STA(k)}{LTA(k)} = \frac{\frac{1}{W_{STA}} \sum_{n=k-W_{STA}}^k |x(n)|}{\frac{1}{W_{LTA}} \sum_{n=k-W_{LTA}}^k |x(n)|}$$

where  $W_{STA}$  is the length of the window for the short-term,  $W_{LTA}$  the length of the long-term, and  $x(n)$  with  $n= 1, 2, \dots, N$  is the amplitude of the signal. Knowing the ratio, we can analyze the signal and determine if an anomalous value exceeds the established thresholds.

### 3.4 Seismic Event Properties

Once seismic events have been identified, it is crucial to classify them based on their properties. Each event has unique temporal, spectral, and amplitude characteristics, which can be quantified using metrics that assign a numerical value to each event. These metrics enable us to differentiate between volcano-tectonic, high-frequency, and explosive events and distinguish between real data and noise. The following temporal, spectral and amplitude metrics and their explanation are based on Kettner & Power (2013).

#### 3.4.1 Temporal Metrics

Temporal metrics measure the data as a function of time (seconds) in different aspects and in different ways to characterize the event. We used three metrics: event length, time between events, and event rate.

##### 3.4.1.1 Length

The difference between the time when the trigger is on and the trigger off. The event duration is directly related to the magnitude of the event.

$$Length = t_{off} - t_{on}$$

Where  $t_{off}$  is the time when the trigger is off; it means the end of the event. The  $t_{on}$  is the time when the event starts. The duration of a volcanic earthquake, also known as the event length, can provide information about the duration of the seismic energy release, which can help determine the type of volcanic activity that produced the earthquake.

##### 3.4.1.2 Gap

The difference in time between the end of one event and the start of the following event, where  $n = 1, 2, \dots, N$  represents the index of the event.

$$Gap = t_{on(n)} - t_{off(n-1)}$$

##### 3.4.1.3 Event Rate

The event rate, represented mathematically as  $E_{rate}$ , is a measure of the frequency of events per hour and is used in the identification of earthquake swarms. The variable  $N_{event}$  denotes the number of events, and the unit of time is specified in hours.

$$E_{rate} = \frac{N_{event}}{time(h)}$$

Seismic activity can indicate the movement of magma and fluids within the volcano, and changes in the rate of earthquakes can indicate changes in the level of activity of the volcano. For example, an increase in the number of earthquakes at a volcano may indicate that an eruption is imminent. Conversely, a decrease in seismic activity may indicate that the volcano is becoming less active. As highlighted by Pesicek et al. (2018), relying solely on the event rate as an indicator of precursor activity may not always be wise.

### **3.4.2 Amplitude Metrics**

The amplitude of a volcano-seismic waveform is a measure of the strength or energy of seismic waves generated by a volcanic eruption. The amplitude is the maximum deviation of the waveform from the average ground motion and is typically measured in units of ground displacement (e.g., millimeters) or velocity (e.g., millimeters per second).

The amplitude of the recorded volcano-seismic waveform is a crucial indicator of the magnitude of the seismic energy released during a volcanic eruption. It provides insight into the size and intensity of the eruption, which can help to better understand the underlying volcanic processes.

#### **3.4.2.1 Maximum Amplitude**

The maximum of the absolute value of the difference between the amplitude and the demeaned amplitude.

$$Max_{amp} = Max \left( \left| x(n) - \frac{\sum_{t_{on}(n)}^{t_{off}(n)} x(n)}{n} \right| \right)$$

The maximum amplitude is the highest deviation of the seismic waveform from its average ground motion and provides a measure of the peak strength of the signal. The maximum amplitude can also be used to distinguish real seismic signals from background noise, as the noise will generally have a much smaller amplitude than a genuine seismic signal.

#### **3.4.2.2 Phase Amplitude**

Phase or peak-to-peak amplitude refers to the difference between the maximum positive and maximum negative amplitudes of a waveform.

$$Phase_{amp} = Max(x(n)) - Min(x(n))$$

The phase amplitude is a measure of the energy contained in a specific frequency band of a seismic signal. Unlike the maximum amplitude, which provides a measure of the peak strength of the signal, the phase amplitude provides information about the distribution of energy across different frequency bands.

### 3.4.2.3 Root-Mean-Square Amplitude (RMS<sub>a</sub>)

The RMS amplitude is a measure of the overall strength of a signal and is calculated as the square root of the average of the squared amplitudes over time. The length of the time window used for the calculation is denoted by W.

$$RMS_a = \sqrt{\frac{1}{W} \sum_{t_{on}(n)}^{t_{off}(n)} x(n)^2}$$

### 3.4.3 Spectral Metrics

The spectral content of a seismic event provides us with valuable information about its frequency characteristics. In spectral analysis, transforming time-domain data to the frequency domain can be achieved through several variations of the Fourier Transform, such as the discrete Fourier transform (DFT), fast Fourier transform (FFT), and short-time Fourier transform (STFT), each tailored to meet specific analysis requirements including data length, computational efficiency, and frequency resolution. By transforming seismic signals from the time domain to the frequency domain, we can analyze the different frequency components present in the waveforms, which is important for distinguishing between low- and high-frequency events. Spectral information is essential for characterizing different types of seismic sources and interpreting the subsurface properties of the Earth.

To convert a time-domain signal to the frequency domain, a Fast Fourier Transform (FFT) is applied to the data after first subtracting the mean value and applying a 10% cosine taper to prevent errors at the edges of the signal. The resulting frequency spectrum contains real

frequency values at discrete frequencies, which are determined by the product of the window size ( $W$ ) and the sampling rate ( $SR$ ) divided by the Nyquist frequency ( $F_{nyq}$ ).

$$F = \left( \frac{F_{nyq}}{W * SR} \right)$$

### 3.4.3.1 Maximum Frequency

Maximum frequency ( $F_{max}$ ) refers to the frequency component of a signal that has the highest amplitude or power, compared to all other frequency components ( $F$ ) present in the signal. In other words, it is the frequency at which the signal is most concentrated or intense.

$$F_{max} = Max(F)$$

### 3.4.3.2 Center Frequency

The center frequency is equivalent to the geometric mean of the lower and upper cutoff frequencies. It is the frequency value at which the sum of the energy (or amplitudes or power) at frequencies above and below are equivalent, within the band from 0 Hz to the Nyquist frequency.  $F_{lower}$  refers to the frequencies below  $i + x$  index and  $F_{upper}$  the frequencies from  $i + x$  to  $w$ , which is the window.

$$F_{center} = min \left( \left| \sum_i^{i+x} F_{lower} - \sum_{i+x}^w F_{upper} \right| \right)$$

The frequency at which the minimum value is obtained is known as the center frequency. The frequency range to be analyzed should be chosen such that the center frequency is in the middle of the final range used.

### 3.4.3.3 Frequency Index

The frequency index is defined as the base-ten logarithm of the ratio between the mean power in the upper spectral band  $A_{upper}$  and the mean power in the lower spectral band  $A_{lower}$ , as proposed by Buurman and West in 2010.

$$FI = \log_{10} \left( \frac{\text{mean}(A_{upper})}{\text{mean}(A_{lower})} \right)$$

The frequency index (FI) is a metric used in volcanic seismology to differentiate between various types of volcanic earthquakes. The FI is based on the ratio of high-frequency energy to low-frequency energy within the seismic signal, allowing for discrimination between earthquakes associated with shallow and deep volcanic processes. The FI is useful for identifying the relative location and nature of the underlying volcanic activity.

In order to calculate the frequency index, it is imperative to establish the lower and upper frequency bounds. The upper and lower bounds should be chosen such that low frequency events primarily have energy in the lower range, and high frequency events primarily have energy in the upper range.

### **3.5 Events Classification**

As we mentioned in section 1.4 there are different seismic signals associated with different types of volcanic events. To identify the type of volcanic event, we will use metrics like Root-Mean-Square amplitude and the Frequency index.

#### ***3.5.1 Type of volcanic event***

For this study, we will consider the most important signals such as Volcano-tectonic (VT), Hybrid (HYB), Long Period (LP) and Explosion earthquakes (EXP). VT events are the primary sign of volcanic activity (Chouet, 1996). The short term increase of VT activity is a good indicator of precursory activity to an eruption. The location of LP events is strongly linked with the movement or any disturbance in the magma flux as well as the interaction of magma and hydrothermal systems. Together, VT and LP events can be used to infer the geometry of the plumbing system of a volcano.

#### ***3.5.2 Manual Classification***

The RMSa is the indicator of the amount of energy released during a seismic event and also indicates any change in the size of the event. When the RMSa value surpasses the pre-established threshold, the type of the volcanic event can be set. The frequency index is the most important metric when we try to classify volcanic events. According to Kettner & Power



(2013) and Buurman & West (2010) low values of FI are indicators of imminent eruptive activity (Explosion earthquakes).

The four types of volcanic events (VT, LP, HYB, and EXP) are typically characterized by different frequency contents and amplitude characteristics. By setting appropriate thresholds, we can classify each event as either low frequency, hybrid, high frequency or explosion. To determine these thresholds, we utilized a "calibration set", with equal representation from each of the three types. We manually selected these events based on the spectral content.

For each event in the calibration set, we performed spectral analysis using Fast Fourier Transform (FFT) applied to the event data. The FFT calculates the frequency content of the event, and we then normalized the amplitude to facilitate comparison between events. Once we set the frequency and amplitude data for the calibration waveforms, we analyzed the resulting data to determine the appropriate thresholds for event classification. This involved examining the distribution of frequency and amplitude for each event type and identifying natural breakpoints in the data that could be used as thresholds. Once the data has been separated into volcano-tectonic, long-period, explosion, and hybrid events, we can begin to analyze each event type and extract relevant information.

### ***3.5.3 Automated Classification***

The previous section provided the background for the automated classification methods used in the analysis of the volcanic events. Even if visual analysis can be used to determine the frequency index (FI) and root-mean-square (RMS) amplitude thresholds, it can be subjective and lead to inconsistencies during classification. Therefore, to reduce subjectivity, statistical calculations and cluster analysis were used to determine the breakpoints for the FI and RMS amplitude. The statistical calculations involves the computation of mean and standard deviation of the data for each event type. Then we use these values to define the thresholds.

Cluster analysis was used to recognize groups of events with similar FI and RMS values. The limits between each cluster can be used as thresholds. This approach helped to reduce the subjectivity of the analysis and ensure consistency in the results. To confirm the reliability of the calculated thresholds, we compared them with the visually-determined thresholds. Overall, the use of statistical calculations and cluster analysis to determine the thresholds for

automated classification of volcanic events provides a more objective and reliable approach than visual analysis alone.

### **3.6 Noise Awareness**

Temporal, amplitude, and spectral metrics can effectively remove much of the noise in seismic data. These metrics include RMS amplitude (RMSa), maximum frequency (MF), phase amplitude (PA), center frequency (CF), length (L), and frequency index (FI), and are established based on Kettner and Power (2013).

To ensure the highest quality data for event location, we will compare the data recorded at multiple stations and keep only the data that has been recorded in at least three stations. Then, for the remaining data, we will use the aforementioned metrics to clean the data and remove any remaining noise.

It is important to note that we do not anticipate any electronic contamination in the data at this stage, as the stations are located far from any infrastructure. However, we will perform additional checks to ensure that the data is free from any interference or contamination.

### **3.7 Swarm Detection**

To gain a better understanding of the relationship between active volcanic and tectonic processes, it is crucial to study the temporal and spatial occurrence of earthquakes (Farrell, J., Husen, S., & Smith, R. B., 2009). Characterizing earthquake swarms, in particular, is essential in this regard. One way to detect earthquake swarms is by using the event rate parameter, which helps identify clusters of events that surpass a specific event rate threshold. To this end, we have implemented an algorithm (see Annex 1) that can accurately recognize such clusters.

### **3.8 VT Events Location**

The most common method for locating volcanic earthquakes is through the use of seismometers, which detect and record the vibrations or seismic waves generated by earthquakes. By analyzing the arrival times and waveforms of these waves at multiple monitoring stations, it is possible to determine the location and magnitude of the earthquake.

For volcano-tectonic earthquakes we will use the grid method, described below, due to its simplicity and we can then map the distribution of seismicity in a volcanic area.

### 3.8.1 Grid Method

The grid method (Gottschämmer & Surono, 2000) will be used to find the location of the VT earthquakes. This method uses location-dependent parameters which require the description or characteristics of the event such as seismic wave velocity, arrival time, etc. To use the grid method, we have to make some assumptions like the waves travel equally in every direction (isotropic radiation), and the medium where the energy is radiated is homogeneous (the seismic wave velocity  $V_p$  is constant).

We define a grid  $P_{mn}$  of  $m \times n$  points over the study area, where the dimension is related to the resolution of the event's location. Once the grid is established, we have to compute the distance of each grid point to the stations, thus obtaining the matrix  $D_{mn}$ .

$$\begin{bmatrix} P_{11} & \cdots & P_{m1} \\ \vdots & \ddots & \vdots \\ P_{1n} & \cdots & P_{mn} \end{bmatrix} \rightarrow \begin{bmatrix} D_{11} & \cdots & D_{m1} \\ \vdots & \ddots & \vdots \\ D_{1n} & \cdots & D_{mn} \end{bmatrix}$$

The number of stations  $N$  has to be equal or greater than two. The location-dependent parameter for VT events is the source time, so we have to calculate a value  $A_{mn}$  for each grid point, where  $A$  is the source time matrix with  $m$ -columns and  $n$ -rows.

In order to compute the source time  $t_{H_{mn}}$ :

$$t_{H_{mn}} = t_{arr} - \frac{D_{mn}}{v_{assumed}}$$

We need to know the seismic wave velocity  $v$ . To get the approximate velocity  $v_{assumed}$ , we will test different velocities. The arrival time  $t_{arr}$  is the time at which the seismic wave is first recorded at a given station.

We will have  $A_{mn_k}$  matrix for each station  $k$ , with entries for each grid point  $mn$ .

$$\begin{bmatrix} A_{11_1} & \cdots & A_{m1_1} \\ \vdots & \ddots & \vdots \\ A_{1n_1} & \cdots & A_{mn_1} \end{bmatrix} \quad \begin{bmatrix} A_{11_2} & \cdots & A_{m1_2} \\ \vdots & \ddots & \vdots \\ A_{1n_2} & \cdots & A_{mn_2} \end{bmatrix} \quad \cdots \quad \begin{bmatrix} A_{11_k} & \cdots & A_{m1_k} \\ \vdots & \ddots & \vdots \\ A_{1n_k} & \cdots & A_{mn_k} \end{bmatrix}$$

So, the calculation has to be done in  $N-1$  stations.

In a perfect scenario where the resolution is high and all the assumptions are true, the source location should agree in every value of the  $A_{mn_k}$  matrix ( $A_{mn_1} = A_{mn_2} = \dots = A_{mn_k}$ ). When one or more of the conditions are not held then the values of the  $A_{mn_k}$  matrix will not agree. For that, we have to approximate the source position using the minimum of the standard deviation:

$$\sigma_{mn} = \sqrt{\frac{1}{N-1} \sum_{k=1}^N (A_{mn_k} - \bar{A}_{mn})^2},$$

Where  $\bar{A}_{mn}$  is the average over all  $A_{mn_k}$ .

Then, we will have a  $\sigma_{mn}$  matrix for each value of  $v_{assumed}$  that we tried.

$$\begin{bmatrix} \sigma_{11_{v_{assumed}}} & \cdots & \sigma_{m1_{v_{assumed}}} \\ \vdots & \ddots & \vdots \\ \sigma_{1n_{v_{assumed}}} & \cdots & \sigma_{mn_{v_{assumed}}} \end{bmatrix}$$

At the end, we have to choose the  $v_{assumed}$  where the overall minimum of the standard deviation occurs. The source location is then chosen as the grid point with the minimum  $\sigma$  value for that  $v_{assumed}$ .

### 3.9 Application

The processing times of the codes are dependent on the computer specifications. In this study, we employed a computer with an AMD E1-6015 APU with Radeon (TM) R2 Graphics 1.40 GHz processor and 4.00 GB RAM. The size of MSEED files for a single day ranges from 9 to 18 MB. The processing time for calculating the STA/LTA ratio and metrics over 1363 MSEED files from five stations was approximately three hours. Upon completion of the initial processing, we obtained CSV files with a size ranging from 1 to 49 KB. The computing time required to locate 1373 VT events over a span of 276 days was 2 hours, 49 minutes, and 30 seconds, resulting in a CSV file with a size of 58 KB.

## 4 RESULTS

We applied the previously described methods to analyze a dataset obtained from Lascar volcano spanning the period of 2014-2015. Our objective was to identify, classify, and accurately locate seismic events within the dataset.

### 4.1 Data

The continuous data were split into days and also into channels (EHE, EHN, and EHZ) to make it more manageable (Figure 5). We downloaded 13145 raw files for the 6 stations and three channels. The stations BB3, BB4, and BB5 operated continuously for four months (April-August) and six months (November-May) with a gap of three months (see Figure 5). On the other hand, BAS, BB1, and BB2 were operative for two years, one year, and eight

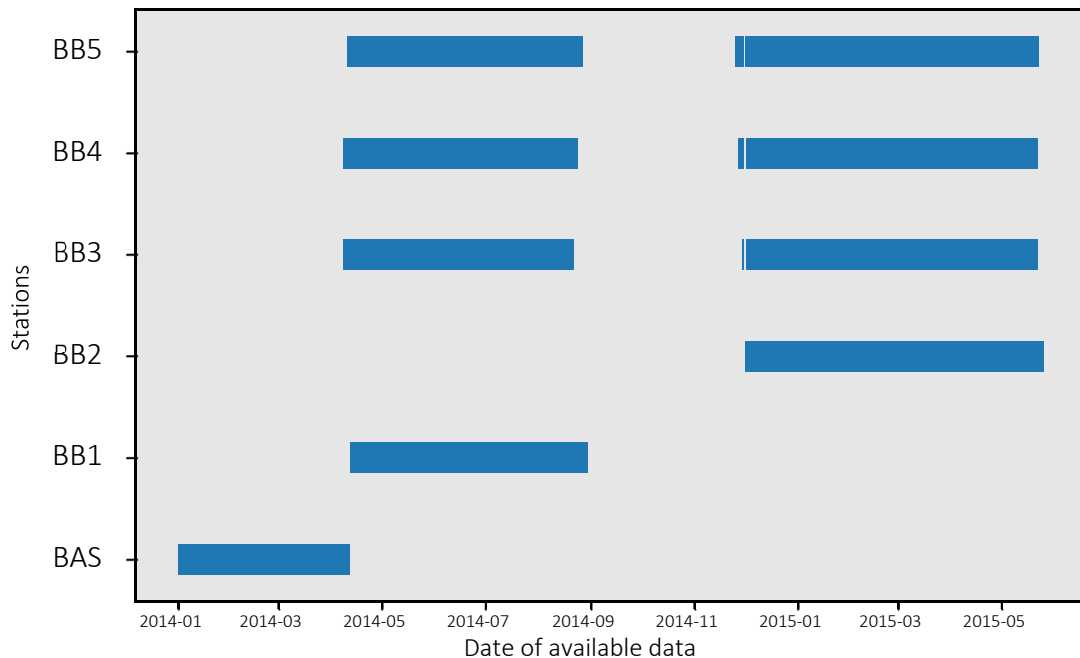


**Figure 5.** Data obtained from GFZ Data Centre for LascarVolcano during 2014-2015

months, respectively. The available data, shown in Figure 5, reveals a gap between August and mostly November of 2014, meaning there is a lack of data during this period. As previously stated, the location method requires data from at least two stations.

## 4.2 Filtering and Downsampling

In this study we applied three techniques: linear detrend, demean detrend, and cosine taper. The cosine taper at 10 % was implemented to minimize spectral leakage, attenuate discontinuities at the signal edges besides, and improves the accuracy of subsequent frequency-domain analyses. To apply the detrending and tapering preprocessing, we utilized detrend and taper functions from Obspy library (Beyreuther et al., 2010; Megies et al., 2011; Krischer et al., 2015 & The ObsPy Development Team, 2022) (See section 4.4, python code (2/5)). Once the data were preprocessed, it was necessary to reduce the sample rate at certain stations which were recorded at 200 Hz; we downsampled those stations to 100 Hz (Figure 6). We applied an anti-aliasing filter (AAF) to avoid aliasing errors during the downsampling (See section 4.4, python code (2/5) for details). However, it also results in a loss of information and limited resolution that can produce artifacts. To mitigate these effects, an antialiasing filter is applied. It smoothens out jagged edges and reduces aliasing by eliminating high-frequency components. After the decimation, we applied a high-pass filter of  $\frac{1}{3600}$  Hz and low-pass filter of 40 Hz. We show an example seismogram before and after

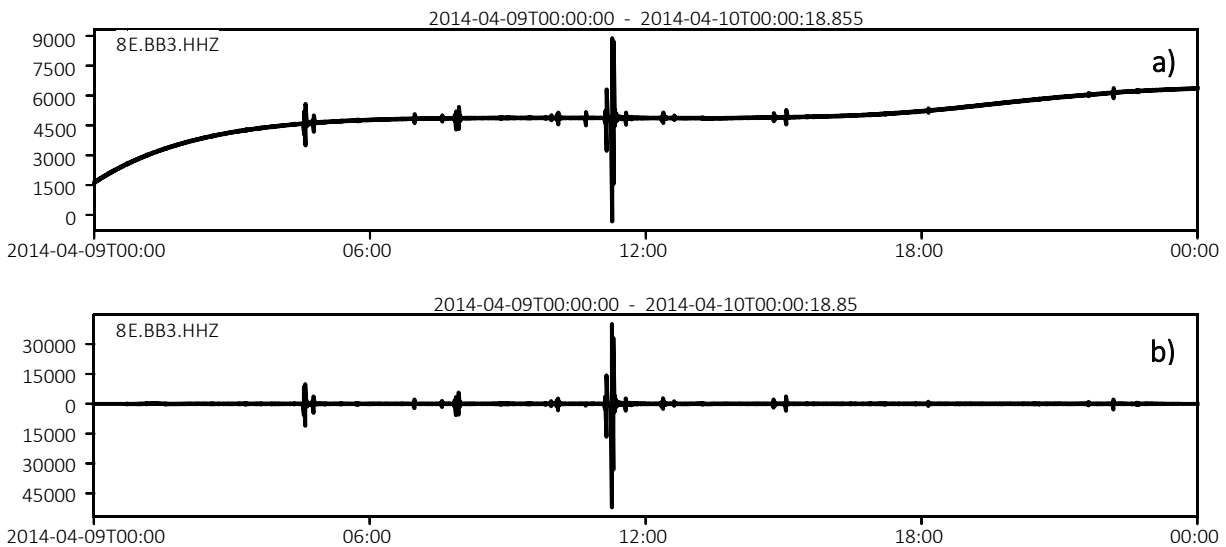


**Figure 6.** Seismic signal recorded in Lascar Volcano April 9th, 2014. a) BB3 station seismogram with a sample rate of 200 Hz without filtering. b) Seismogram of processed data (downsampling/decimation) with a sample rate of 100 Hz. The data was filtered with a high-pass filter of  $\frac{1}{3600}$  Hz and low-pass filter of 40 Hz.

the preprocessing (Figure 6a). The downsampling and filtering of the signal helps remove high-frequency noise components (Figure 6b).

### 4.3 Identification of Seismic Events

Filtering is vital since the preprocessed data may still contain noise. To address this issue, various filters ranging from 0.0003 to 40 Hz were applied to the data (Figure 7). Upon visual inspection, it was noted that a bandpass filter between 0.2 to 10 Hz was effective in attenuating most of the noise; however, not all the signals were detected. As a result, a narrow band filter between 1 to 10 Hz was implemented exclusively for the purpose of the STA/LTA

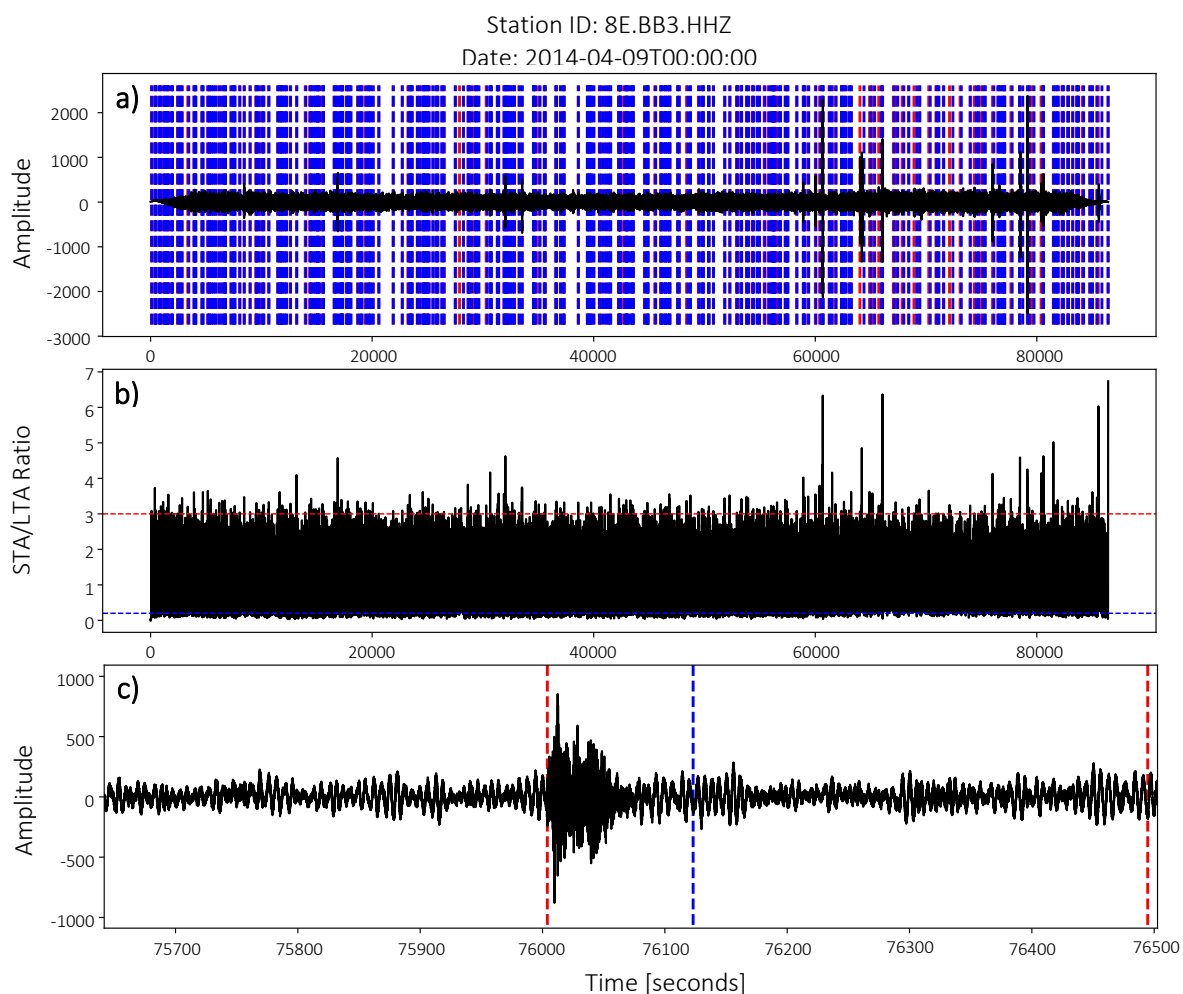


**Figure 7.** The STA/LTA ratio is displayed graphically as follows: a) Seismogram from April 9, 2014 of Lascar volcano, with the red dashed line indicating the moment the STA/LTA ratio crosses the upper threshold, and the blue dashed line marking the lower threshold. b) The STA/LTA values for the April 9th, 2014 seismogram are shown. c) A close-up view of one anomaly identified by the STA/LTA method between 21:06:40 and 21:08:20 on April 9, 2014.

calculation (see Figure 7). It is pertinent to note that the antialiasing, cosine tapering, and ‘demean’ and ‘linear’ detrending noise removal techniques will be employed for all further analyses.

The Short-Term Average Long-Term Average (STA/LTA) method was implemented using a  $W_{STA}$  of 1 second and  $W_{LTA}$  of 7 seconds. Once we had the STA/LTA ratio we established a ‘trigger on’ of 3.1 and a ‘trigger off’ of 0.2. If the ratio surpassed the trigger, the time of the anomaly will be recorded in a new list as **Ton**. When the ratio next dips below the trigger off threshold (Figure 7b), the time will be saved in the **Toff** (see Section 4.4.1 for calculation details). A comparison between the events recorded in the seismogram and those identified by the method reveals that the locations of the red and blue dashed lines correspond to the seismic events visually identified. The anomalies in the STA/LTA ratio will be considered as seismic events (Figure 7b, c). Each value that exceeds the upper threshold will mark the beginning of a seismic event, while the lower threshold will signify the end of the previously identified event.

#### 4.4 Seismic Event Properties

After identifying the seismic events at Lascar, it is important to describe and characterize each event using relevant metrics. Nine metrics were used in our analysis: event duration (length), time between events (gap), number of events per unit time (event rate), peak amplitude (maximum amplitude), average amplitude of a waveform's oscillation (phase amplitude), root mean square amplitude (RMSa), highest frequency in the frequency spectrum (maximum frequency), central frequency of the frequency spectrum (center frequency), and a measure of the frequency content of the waveform (frequency index). The event properties were characterized using nine metrics as well as the STA/LTA ratio and are detailed in the Python code block.



#### 4.4.1 Metrics calculation Python code

The following Python code is used to process Lascar volcano seismic data from January 1st, 2014 to December 31, 2015. It pre-processes the seismic signals, calculates the STA/LTA ratio, the initial and end times for the events, and the nine metrics described in section 3.3.

```
#=====
from scipy.fft import rfft, rfftfreq
from timeit import default_timer as timer
from datetime import timedelta
start = timer()
from Thesis_3_4 import sta_lta, t_on_off
from obspy import read
import numpy as np
import pandas as pd
#=====
#=====

network = '8E'
channel = 'HHZ'
stations = ['BAS', 'BB1', 'BB2', 'BB3', 'BB4', 'BB5']
fday = 1 # start day
eday = 31 # end day
fmonth = 1 # start month
emonth = 12 # end month
year = ['2014', '2015']
#=====

for y in year:
    year = str(y)
    for s in stations:
```

Continue... (0/5)

```

station = str(s)

for k in range(fmonth, emonth + 1, 1):

    month = str(k)

    for a in range(fday, eday + 1, 1):

        day = str(a)

        try:

# Set the directory to get the mseed files, these files were previously
# downsampled. All data have a sampling rate of 100 Hz

            file = '{}.{}.{}.{}{}{}.mseed'.format(*[network,
station, channel, year, month.zfill(2), day.zfill(2)])

            st = read(file)

# Apply the pre-processing techniques: Linear detrend, demean detrend, and
# the cosine taper at 5%

            st.detrend(type='demean')
            st.detrend(type='linear')
            st.taper(type="cosine", max_percentage=0.05)

# Implement a low-pass filter at 0.4 times the sampling rate, and a high-
# pass filter to attenuate signals below 1/3600 Hz to avoid aliasing
# artifacts.

            st.filter('lowpass', freq=0.4 * 100, zerophase=True)
            st.filter('highpass', freq=1 / 60 / 60,
zerophase=True)

# Once the data is prepared we created a copy to be used in the metrics
# calculation section

            st1 = st.copy()

```

Continue... (1/5)

# The pre-processed data is filtered again using a low- and a high-pass filter just for the STA/LTA ratio calculation. The cutoff frequencies were established based on the characteristics of the waveforms and testing different values.

```
st.filter('lowpass', freq=10, zerophase=True)
st.filter('highpass', freq=1, zerophase=True)
tr = st[0]
print(file)
data1 = np.array(tr.data)
npts = tr.stats.npts
sr = tr.stats.sampling_rate
time = np.arange(npts, dtype=np.float32) / sr
```

# Set the windows for the STA and LTA calculation. The time window is in seconds so we have to multiply it by the sampling rate.

```
nsta = int(1 * sr)
nlta = int(7 * sr)
sta = sta_lta(data1, nsta, nlta)
```

# Set the thresholds where the ratio is considered as event trigger. When the STA/LTA ratio is up to 3.1 the time of occurrence will be saved as the initial time of the event. In the same way the tOff is the lower threshold, ratios below 0.4 will be saved as the end time of the event.

```
tOn = 3.1
tOff = 0.4
triggers = t_on_off(sta, tOn, tOff)
t_on = triggers[:, 0]
t_off = triggers[:, 1]
```

# The data from now and on is not affected by the low- and high-pass filter used by the STA/LTA analysis. In this way, the metrics values will contain all the information and characteristics that could be deleted during filtering.

```
tr = st1[0]
data = np.array(tr.data)
npts = tr.stats.npts
sr = tr.stats.sampling_rate
time = np.arange(npts, dtype=np.float32) / sr
```

Continue... (2/5)

```

max_freq = [] # Maximum Frequency
cf = [] # Central Frequency
FI = [] # Frequency Index
RMS = [] # RMS Amplitude
max_amp = [] # Maximum Amplitude
p_amp = [] # Phase Amplitude

#=====
# The following section will calculate the metrics values for each event
recognized by the STA/LTA ratio. All the values will be saved in the empty
lists described above.
#=====

length = np.divide((t_off - t_on), sr)
gap = [(t_on[i+1] - t_off[i])/sr for i in
range(len(t_on)-1)]

# The p value is the desired time window for the rate in this case will be
one hour in seconds times the sample rate.

c = [[]]
p = 360000
while p <= len(data) - 360000:
    for i in t_on:
        if i > p - 360000 and i <= p:
            c[-1].append(i)
        c.append([])
    p += 360000

event_rate = [len(e) for e in c]

# For the following steps, the edata variable represents the amplitude
data for one event.

for s in range(0, len(t_on), 1):

    edata = data[t_on[s]:t_off[s]]

    # Calculate the RMS amplitude

    rms_amplitude =
np.sqrt(np.mean(data[t_on[s]:t_off[s]] ** 2))

```

Continue... (3/5)

```

RMS.append(rms_amplitude)

# Calculate the maximum amplitude

demean = edata - np.mean(edata)

pa = max(abs(demean))

max_amp.append(pa)

# Calculate the phase-amplitude

pamp = max(edata) - min(edata)

p_amp.append(pamp)

#=====

# This is the FFT calculation to transform from the time domain to the
frequency domain. The Maximum frequency, Phase frequency, Center frequency,
and the Frequency Index will be computed according to the frequencies
calculated by FFT. To compute the FFT we use the demean data since the
data is concentrated around zero.

#=====

fft_signal = rfft(demean)

freqs = rfftfreq(len(demean)) * sr

# Calculate the maximum frequency

m_freq = freqs[np.argmax(np.abs(fft_signal))]

max_freq.append(m_freq)

# Calculate the center frequency and frequency
index

freq_sum = np.cumsum(np.abs(fft_signal))

center_freq = freqs[np.argmin(np.abs(freq_sum -
freq_sum[-1] / 2))]

cf.append(center_freq)

upper_amp = np.mean(np.abs(fft_signal[freqs >
center_freq]))

lower_amp = np.mean(np.abs(fft_signal[freqs <
center_freq]))

Continue... (4/5)

```

```

        freq_index = np.log10(upper_amp / lower_amp)
        FI.append(freq_index)

#=====
# This section is used to save the trigger times and metrics calculated
# above and saves it in a CSV file.
#=====

        dfton      =      pd.DataFrame(list(zip(*[t_on])),
columns=['Trigger_on'])

        dftof      =      pd.DataFrame(list(zip(*[t_off])),
columns=['Trigger_off'])

        df1        =      pd.DataFrame(list(zip(*[length])),
columns=['Length'])

        df2        =      pd.DataFrame(list(zip(*[gap])),
columns=['Gap'])

        df3        =      pd.DataFrame(list(zip(*[event_rate])),
columns=['Event_Rate'])

        df4        =      pd.DataFrame(list(zip(*[max_amp])),
columns=['Maximum_Amplitude'])

        df5        =      pd.DataFrame(list(zip(*[p_amp])),
columns=['Phase_Amplitude'])

        df6        =      pd.DataFrame(list(zip(*[RMS])),
columns=['RMS_Amplitude'])

        df7        =      pd.DataFrame(list(zip(*[max_freq])),
columns=['Maximum_Frequency'])

        df8        =      pd.DataFrame(list(zip(*[cf])),
columns=['Center_Frequency'])

        df9        =      pd.DataFrame(list(zip(*[FI])),
columns=['Frequency_Index'])

        df = pd.concat([dfton, dftof, df1, df2, df3, df4, df5,
df6, df7, df8, df9], axis=1)

        df.to_csv({}.{}.{}.{}{}{}.csv'.format(
            *[network, station, channel, year, month.zfill(2),
day.zfill(2)]))

    except FileNotFoundError:

        pass

end = timer()

print(timedelta(seconds=end - start))

#=====

```

(5/5)

#### ***4.4.2 Identified Events***

The Python code used to calculate metrics generated 1362 CSV files, one for each day recorded at the five stations (BAS, BB1, BB2, BB3, BB4, and BB5). Each file contains the values for variables such as arrival time, station, date, event type, frequency index, length, gap, maximum amplitude, phase amplitude, RMS amplitude, maximum frequency, center frequency, and event end times. After merging all data from all stations and event types, we identified 127028 events.

All of the identified events were detected using the STA/LTA ratio without any noise removal process applied to eliminate signals that do not meet the predefined ratio threshold. This approach carries the risk of including false positives or extraneous signals that are not related to the actual events, but it also ensures that no true events are missed due to overly aggressive noise removal.

#### **4.5 Events Classification**

We classified the identified events first using manual classification, then automated classification, as detailed below.

##### ***4.5.1 Manual Classification***

To classify the signals, we employed a "calibration set" comprising 120 events. We analyzed the frequency content, as well as the various metrics and ratios of these events to establish thresholds for noise removal and automatic classification. By using this calibration set, we will be able to accurately classify the signals into their respective events.

To visually classify the seismic signals, we analyzed the frequency distribution of 15 events by plotting their Normalized Spectral Amplitude against frequency content. This approach allowed us to categorize the signals based on their frequency content and visually compare the different clusters. Overall, this technique provided a clear and concise way to present the results of our analysis and helped us better understand the frequency content of each signal.

We analyzed the spectral amplitude over frequency for 15 signals, highlighting the identified peaks (Figure 8). We classified the signals into three clusters based on their frequency content: the lower frequency band is concentrated between 0 to 2 Hz, the high frequency band is concentrated above 10 Hz with significant peaks between 5 and 9 Hz, and the hybrid

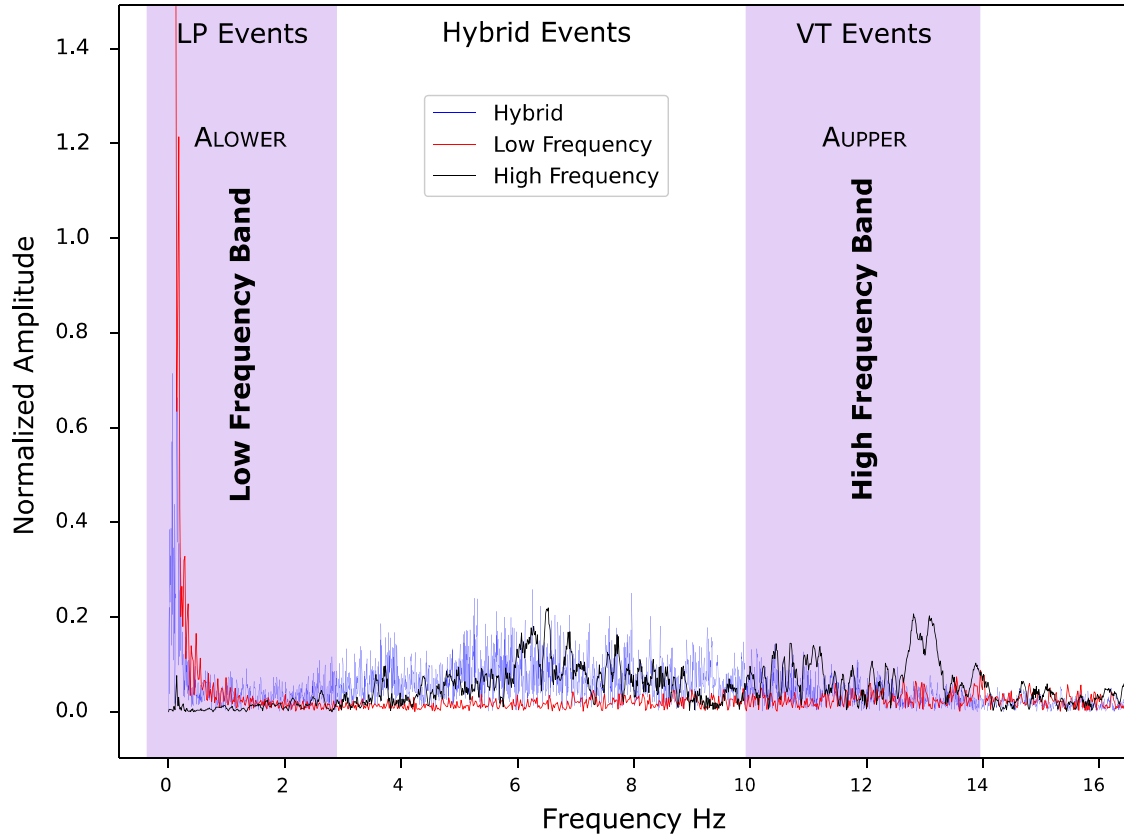


**Figure 8.** Frequency bands determination for visual classification. 15 events were separated into 3 frequency-based clusters: red for low frequency, black for high frequency, and blue for mixed frequency signals.

signals have significant single peaks around 0 Hz with peaks concentrated between 5 to 9 Hz (Figure 8).

It is important to note that in previous steps, we removed trends using linear and demean detrend for the entire dataset. However, during this step, we noticed that most of the signals had unusually high peaks at zero. These artifacts can occur when the signal is not centered on zero, and the FFT includes large DC (direct current) components in the frequency spectrum, which can obscure other frequency components and make it difficult to interpret the spectrum. To address this issue, we computed the FFT using data specifically demeaned for each event instead of the original data detrended by day.

By doing so, we were able to center each signal on zero, effectively removing the DC component and making it easier to identify other frequency components. This approach



improved the accuracy and interpretability of the frequency spectra, allowing us to identify and analyze the significant peaks more effectively.

The manual classification of the 120 events were made based on the frequency bands established before. Following the manual classification parameters we identify low frequency events (Figure 9). The low frequency signal was studied based on its normalized spectral amplitude (NSA), where this signal shows NSA values ranging from 0 to 2.0 in the lower frequency band (Figure 9a). On the other hand, the NSA values in the upper frequency band tends to 0.1, which is considered a very low value (Figure 9a). The FI values for low frequency events are often below -1 and the RMS amplitude keeps in a low range (Figure 9a). The duration of this event type is very variable, ranging from seconds (Figure 9a) to minutes. The shape of the low-frequency event in the time domain does not represent a

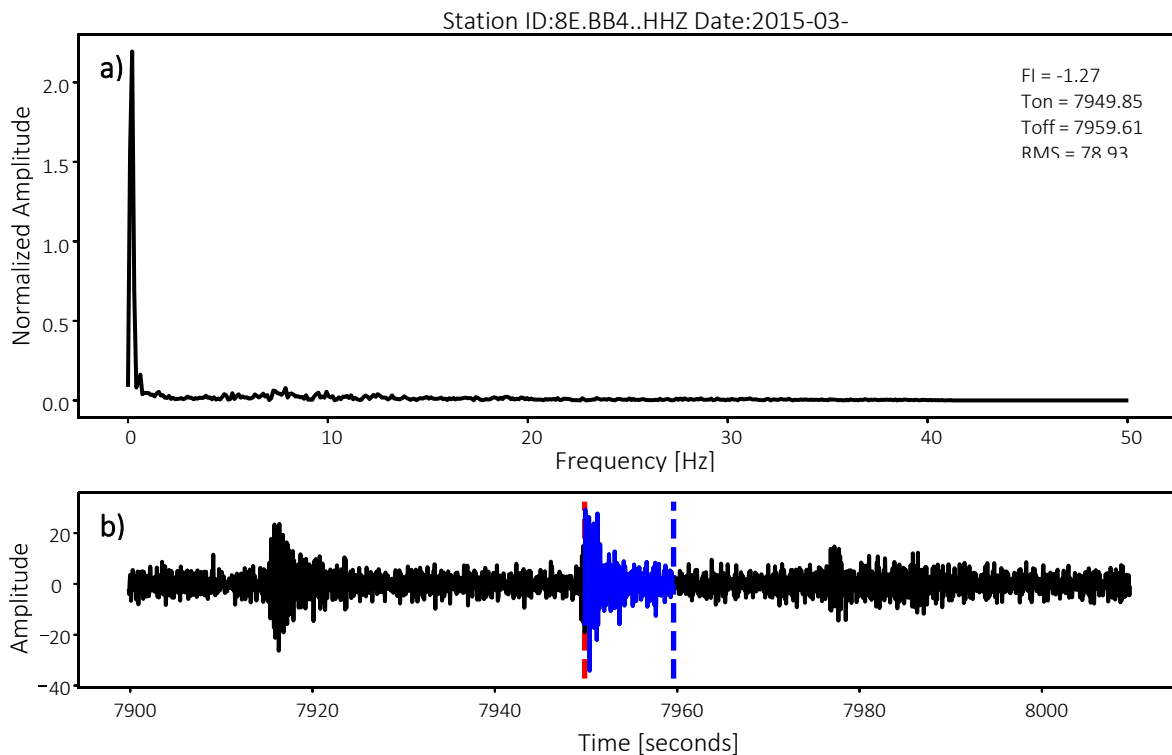


**Figure 9.** Manual classification example for low frequency events. This event occurred in March 4, 2015 recorded at BB4 station. a) Normalized spectral amplitude over frequency. The description of the event like FI, RMSa, Ton, and Toff are described in the upper right corner. b) Amplitude over time. The amplitude data for the event are presented in blue. The red line represents the beginning of the events and blue dashed line the end of the event.

determinant parameter to differentiate low-frequency events from high-frequency events (Figure 9b). The LF signal can be enhanced by the application of a specific filter, but it can pose a problem when attempting to automatically classify LF events because the filters may vary between LF signals. Applying the manual classification parameters we add high frequency events to the calibrations set (Figure 10). The NSA values for this event are very low, ranging from 0 to 0.25 (Figure 10a). In the low frequency band, the maximum value for NSA reaches only 0.23 in a single peak very low to be considered as an LP or HYB event. However, as the frequency increases, the NSA values and the numbers of peaks gradually increase and become significant at around 7 Hz (Figure 10a). The waveform shows the abrupt onset with a sharp increase in amplitude followed by a rapid decay (Figure 10b). This waveform pattern is typical of high frequency events.

The seismic events that were classified as hybrid events, display characteristics of both high-frequency and low-frequency signals in the frequency spectrum, as expected (Figure 11). The

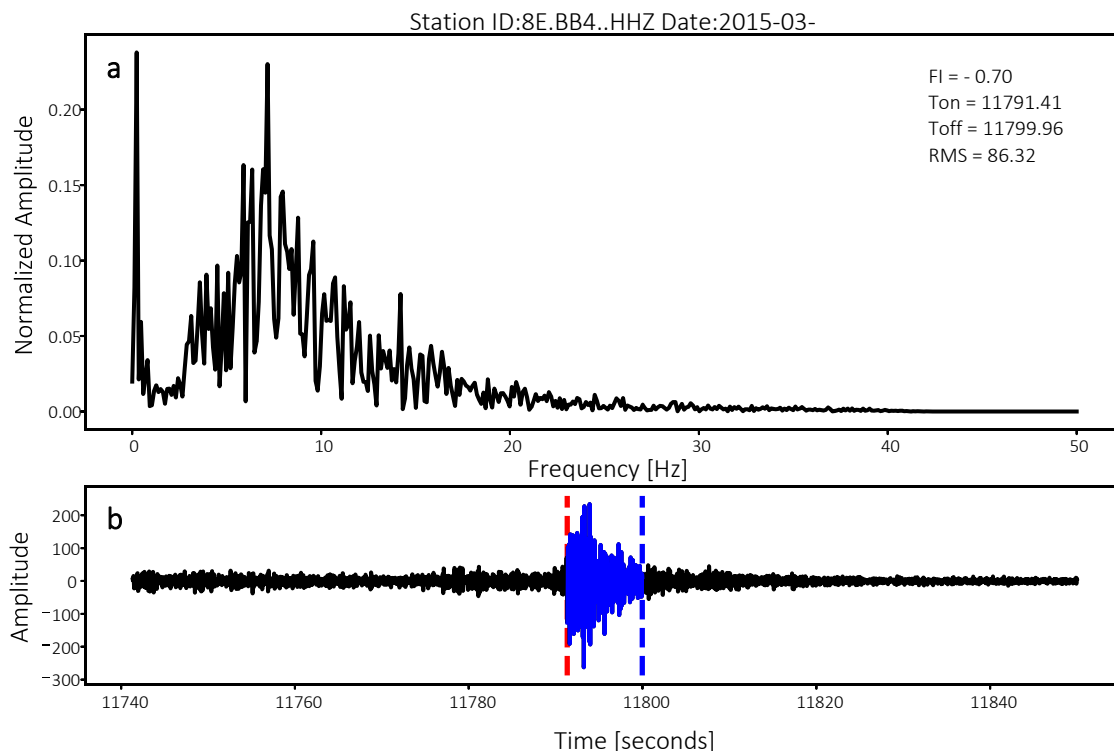


**Figure 10.** Manual classification example for high frequency event. This signal was recorded on March 4, 2015 at BB4 station. a) Normalized spectral amplitude over frequency domain. b) Amplitude over time for the event occurred from 03:16:31 to 03:16:40.

high- and low-frequency signal characteristics are more evident in the NSA values. When examining the lower frequency band, the NSA is higher compared to VT events but similar to LP events (Figure 11a). We have noticed that the NSA values in the low-frequency band of hybrid events usually range from 0.7 to 1.6. On the other hand, NSA values in the upper band are not as low as in LP events, with significant peaks ranging between 2.5 and 7 Hz and positioned between the lower and upper bands.

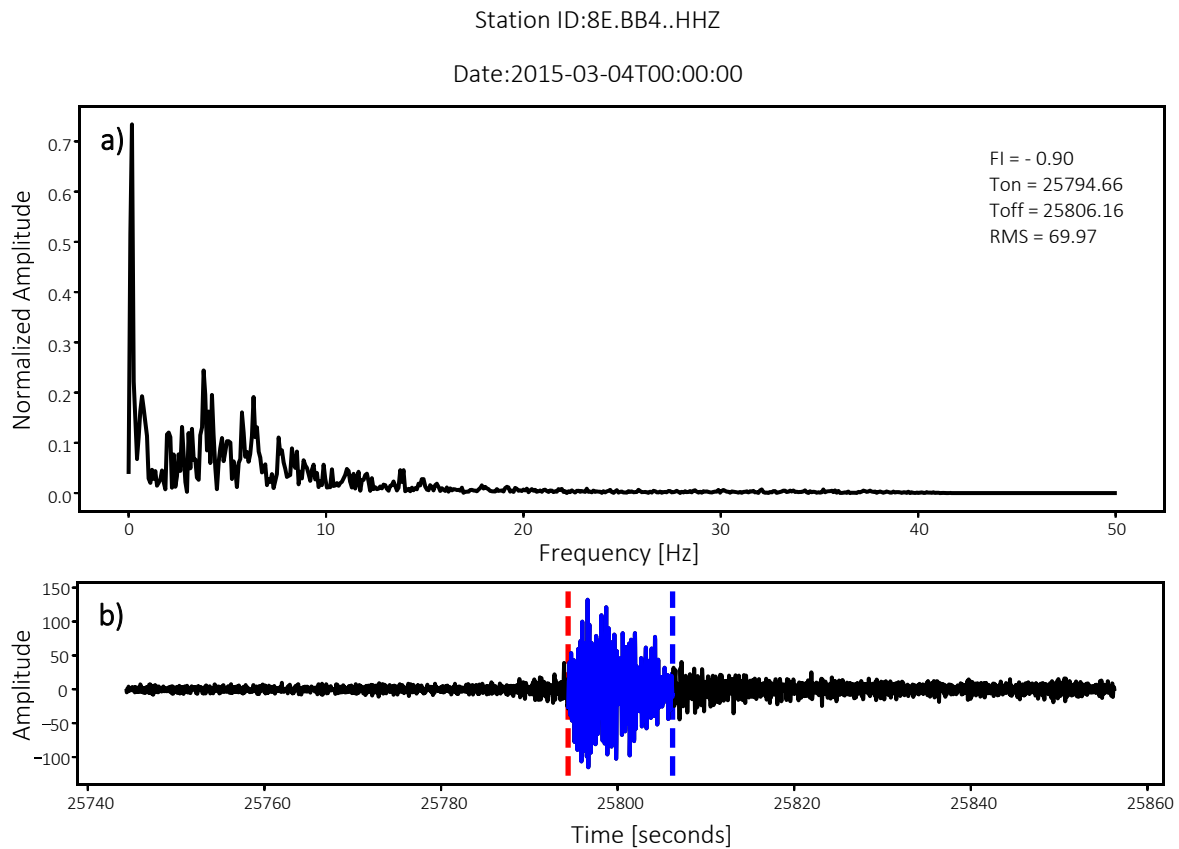


**Figure 11.** Manual classification example for hybrid events. The exemplified event was recorded at Lascar on March 4, 2015. a) Normalized spectral amplitude over frequency with a maximum NSA at lower frequencies. b) Amplitude over time of an event occurred at 07:09:54 and end at 07:10:06.

Analyzing the waveform for a hybrid event, it is difficult to distinguish the high-frequency beginning followed by the low-frequency part of the event in the waveform (Figure 11b). This waveform can be easily confused as a low-frequency event, but the spectral distribution contains both types of signals. Therefore, the analysis of hybrid events based on the frequency content is essential for accurate classification.

The waveform of hybrid events can be difficult to interpret, as it can resemble that of LP or VT events. However, the spectral content can help to distinguish between these different types of events. Hybrid events typically display a spectral distribution that contains both high- and low-frequency components, with a dominant low-frequency component. The FI is consistent with the values observed for the majority of VT and LP events. Even if the FI value is correctly classifying the event the RMSa do not match with expected values. To improve the accuracy of the classification method we can include more metrics like length since the FI and the RMS metrics are affected by the duration of the event.

During manual classification, we observed some patterns in the FI distribution that were related to different types of events. Based on visual analysis, we determined that the majority of low frequency events (which accounted for over 50% of the identified events) were characterized by FI values ranging from -2.3 to -0.9. On the other hand, high frequency events had FI values above -0.7 and below 1. For hybrid events, determining the thresholds was more difficult since the events were widely distributed, with confusing FI and RMS values. However, even with the spread of values, a pattern still emerged, with RMS values falling between 100 and 200. For hybrid events, the FI thresholds were determined by the LF and HF signals, since these events are in the middle of the frequency bands. The FI ranges from -0.9 to -0.7.

#### ***4.5.2 Automated Classification***

Automated classification involves performing basic statistical calculations and cluster analysis. In order to determine the FI thresholds, we computed the mean value and standard deviation for the three types of events from our calibration set (Table 2). For the LF threshold, we subtracted three times the standard deviation from the mean value, and we followed the same process for the HF thresholds. To determine the lower threshold for Hybrid events, we added one standard deviation to the LF mean. To determine the upper threshold, we added one standard deviation to the HF mean.

After defining the FI thresholds, the next step is to determine the thresholds for the RMS values. We employed k-means cluster analysis to set the thresholds for the RMS amplitudes using the calibration set (Figure 12). In addition to RMSa, we also considered the event type during clustering. As a result, we established thresholds for LF, HF, and HYB events.

Specifically, the threshold between LF and HYB is set at 150, while the threshold between HYB and HF is set at 290 RMS. Although most of the data falls within the predetermined clusters, not all of it does. Therefore, we may need to apply additional filters or metrics combinations for even better classification.

**Table 2.** Statistical description for the FI threshold calculation. EXP are below LF lower threshold.

Type	Mean	Standard Deviation	Lower Threshold	Upper Threshold
Low Frequency	-1.2327	0.3212	-2.1974	-0.9115
Hybrid	-0.8477	0.1308	-0.9115	-0.7686
High Frequency	-0.6867	0.3212	-0.7686	-0.4412

The seismic events with extremely low FI values ( $< -2.2$ ) were categorized as explosion earthquakes, as they do not conform to the LP classification criteria based on FI. However, upon analyzing the amplitude characteristics such as RMSa, maximum amplitude, and phase

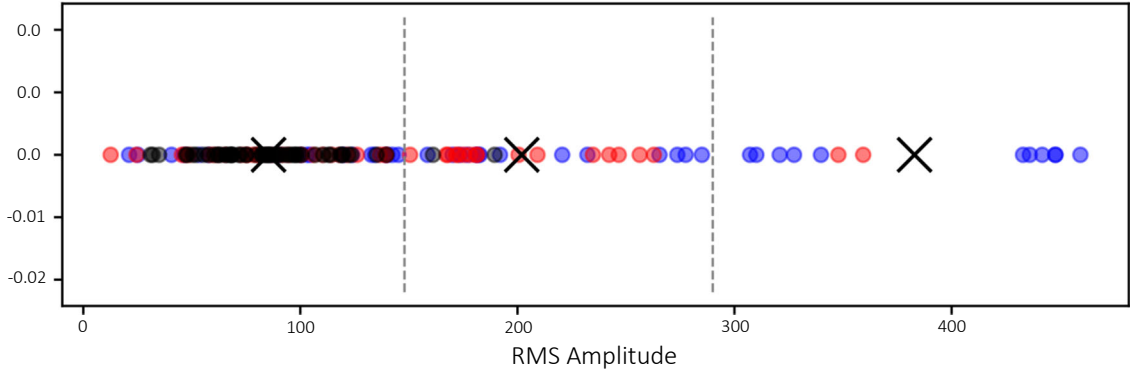


**Figure 12.** K-means cluster analysis for RMS amplitude values of the calibration set. The center of each cluster is denoted by an X, and the gray dashed lines represent the thresholds. The low frequency events are represented by black dots, while the hybrid frequency and high frequency events are denoted by red and blue dots, respectively.

amplitude, this classification remains consistent. While the EXP classification is applicable in our current dataset, it should not be considered a reliable methodology for future

classification of explosion events. This is due to the infrequent occurrence of explosion quakes in our dataset, which limits the generalizability of the EXP classification approach.

### 4.5.3 Identified and Classified Events

After establishing the thresholds for FI and RMS amplitude, we were able to classify the entire dataset into four categories: high frequency, low frequency, hybrid, and explosion events (Figure 13). The analysis revealed that the dataset contained a total of 127,028 seismic events, including 75,509 Volcano-Tectonic events, 32,687 Long Period events, 17,749

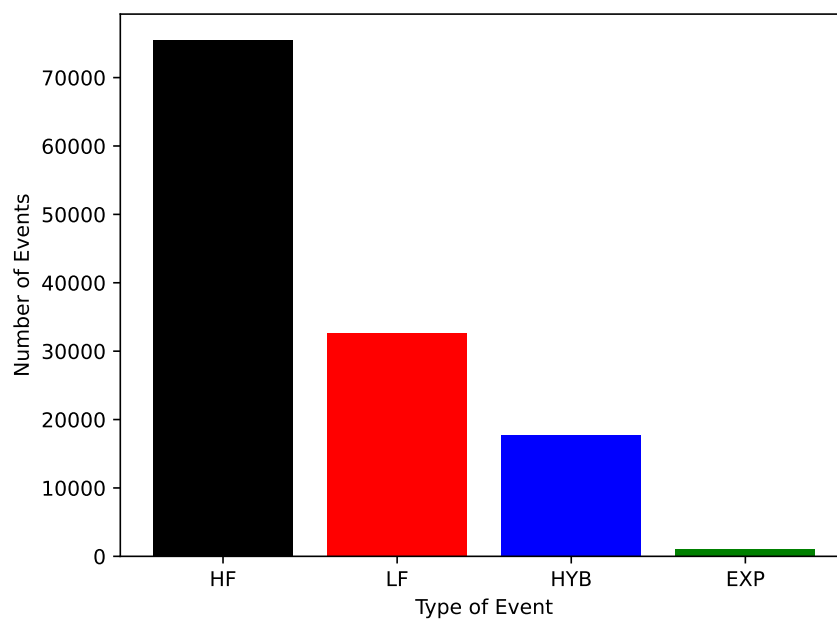


**Figure 13.** During 2014-2015, events were identified at Lascar volcano, including 75,509 high frequency events, 32,687 low frequency events, 17,749 hybrid events, and 1,083 explosion events.

Hybrid events, and 1,083 signals classified as explosion events.

### 4.6 Noise Awareness

The strategies for removing noise from the BAS station and the BB1 to BB5 stations differ, as the noise in the latter group can be more easily identified and removed by comparing recognized events between stations. To identify signals as events, we developed a Python code called Event Recognition (see Annex 1), which analyzes the datasets from the five stations based on their arrival times, dates, and stations. Specifically, a signal must occur

within a 1.5-second window, have the same date, and be recorded in at least three different stations to be considered an event.

Using the method described before, we identified a total of 2951 events, out of which 1373 were classified as high frequency, 984 as low frequency, 588 as hybrid, and 6 as explosion events. This approach helps eliminate much of the noise in the data, but may also result in some loss of valuable information. Nonetheless, the data quality remains high enough to use for event location.

In contrast, the data from the BAS station is unique to the period of January to April 8, 2014, so the above strategy cannot be applied. Instead, we employed metrics calculations to remove noise for single station detection (SSD). The thresholds and metrics used were defined by the calibration set (Table 3). Specifically, we used length (L) phase amplitude (PA), RMS amplitude (RMSa), maximum frequency (MF), center frequency (CF), and frequency index (FI) as the metrics to help clean the BAS dataset of 9266 events.

Table 3 shows that 4723 noisy signals were removed from a dataset of 9266, leaving a total of 4543 resulting events. These noisy signals were identified and removed using the BAS noise removal strategy described earlier. By applying these metrics, we were able to reduce

**Table 3.** SSD Noise thresholds determination for BAS station

Metrics Criteria	Noisy signal	Removed Noisy Events	N° Events
RMSa < 10	1251	1251	8015
MF < 0.05 Hz	170	30	7985
MF > 17 Hz	3483	3304	4681
PA/RMSa > 25	394	138	4543
CF/PA > 120	177	0	4543
FI > 0.4412	41	0	4543
L < 2 seconds	0	0	4543

the noise and improve the quality of the data.

To conduct a more detailed analysis, we applied the single-station detection (SSD) method for each station (for details see Annex 2). After removing noisy events, we identified a total of 113,992 events. Details on the total numbers of events before and after noise filtering can be found in Annex 3.

#### 4.7 Filtered Events

After classifying and filtering the identified events, we randomly selected a few examples of various types of events found at Lascar volcano. It is worth noting that this section does not include all types of events that were identified during our analysis. Nonetheless, these selected examples provide valuable insights into the nature and characteristics of the seismic activity at the volcano.

An example of an event identified during our analysis is the Volcano-Tectonic event that occurred at Lascar volcano on August 11, 2014, at 04:51 AM (see Figure 14). Volcano-Tectonic signals are typically characterized by sharp and impulsive waveforms, characterized by a sudden increase in amplitude followed by a rapid decrease. This particular event had a duration of approximately 40 seconds. Analysis of the spectrogram revealed that the majority

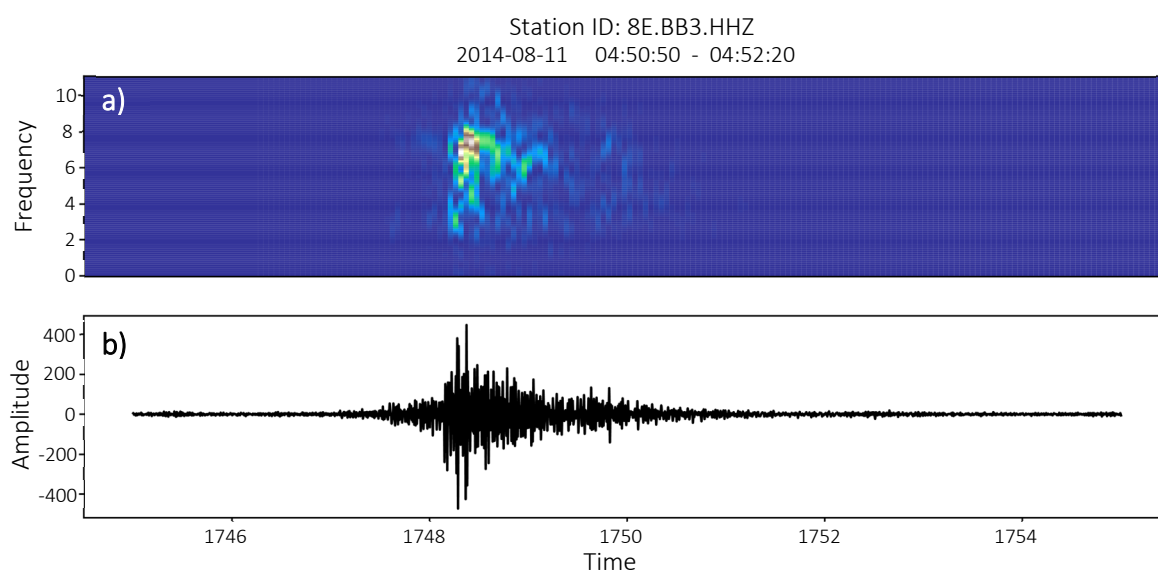


**Figure 14.** Volcano-Tectonic signal recorded at Lascar Volcano in station 8E.BB3 on August 11, 2014 at 04:50. This event was filtered using a band-pass filter between 0.2 to 10 Hz. a) Spectrogram for VT event, where lowest values are represented by blue and highest by white. b) Seismogram for VT event recorded in HHZ channel.



of the energy was concentrated between 5 to 9 Hz. Furthermore, there was a gradual decrease in energy over the subsequent seconds.

Hybrid events are a complex type of seismic signal that exhibit characteristics of both volcano-tectonic (VT) and long-period (LP) events. We identified an event that serves as a clear example of a hybrid signal, which occurred on August 11, 2014, at 04:48 in the morning (Figure 15). The spectrogram of the hybrid signal does not show significant changes in the frequency content. This particular hybrid event had a duration of approximately four minutes, showcasing the prolonged and diverse nature of hybrid signals.

We can observe a sharp change at the onset of the record, followed by a gradual decrease in amplitude. After approximately 20 seconds, the amplitude begins to increase once more. The spectrogram reveals two distinct phases in the frequency distribution. Initially, the majority of the energy is concentrated in the low-frequency band (below 5 Hz). However, as the event progresses, the energy gradually spreads to the higher frequency band, ultimately peaking at around 10 Hz. This event is an intriguing example of seismic activity at Lascar volcano and provides valuable insights into the complex nature of volcanic activity.

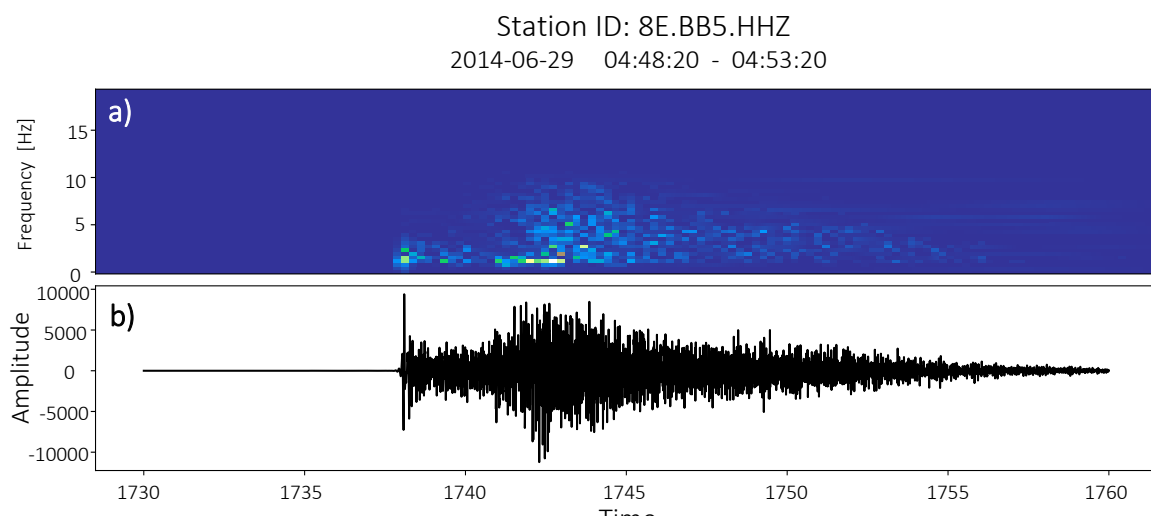


**Figure 15.** Hybrid signal identified at Lascar on August 11, 2014 at 04:48 in the morning. This event was filtered between 1 and 10 Hz. a) Spectrogram for HYB event with a minimum frequency varying from 0.2 to approximately 5 Hz at the beginning of the signal, then reaching a frequency of 10 Hz. b) Seismogram of HYB event recorded in HHZ channel.

Another event identified during our analysis was a low-frequency or long period (LP) event picked up by station 8E.BB2 on December 03, 2014, at 22:51 (Figure 16). Unlike Volcano-Tectonic events, long period events have an emergent onset and the energy decreases gradually over time. The low-frequency signal had a duration of approximately 16 seconds. The spectrogram shows that the frequency content of this LP event varied from 0.2 to 7 Hz (Figure 16a).

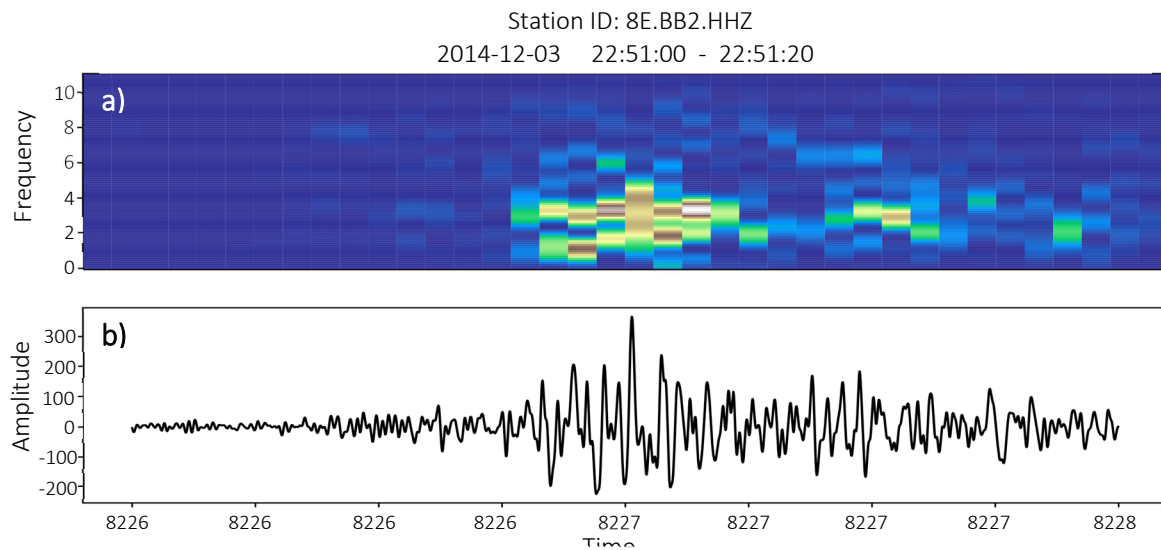


**Figure 16.** Low-frequency signal recorded at Lascar Volcano on December 3, 2014 at 22:51. The LP event was filtered using a band-pass filter between 0.2 and 10 Hz. a) Spectrogram for LP event with a minimum frequency varying from 0.2 to approximately 5 Hz. b) Seismogram of LP event recorded in HHZ channel.

While this study specifically focuses on analyzing LF, HF, EXP, and HYB signals, it's worth noting that other types of signals exist, such as very low frequency (VLF) events and tremors. VLF events (Figure 17) are associated with Strombolian eruption activity, and can be caused by pressure changes resulting from gas and magma intrusions. Therefore, although not directly studied here, VLF signals are important to consider in our understanding of volcanic activity as well as other seismic signals.

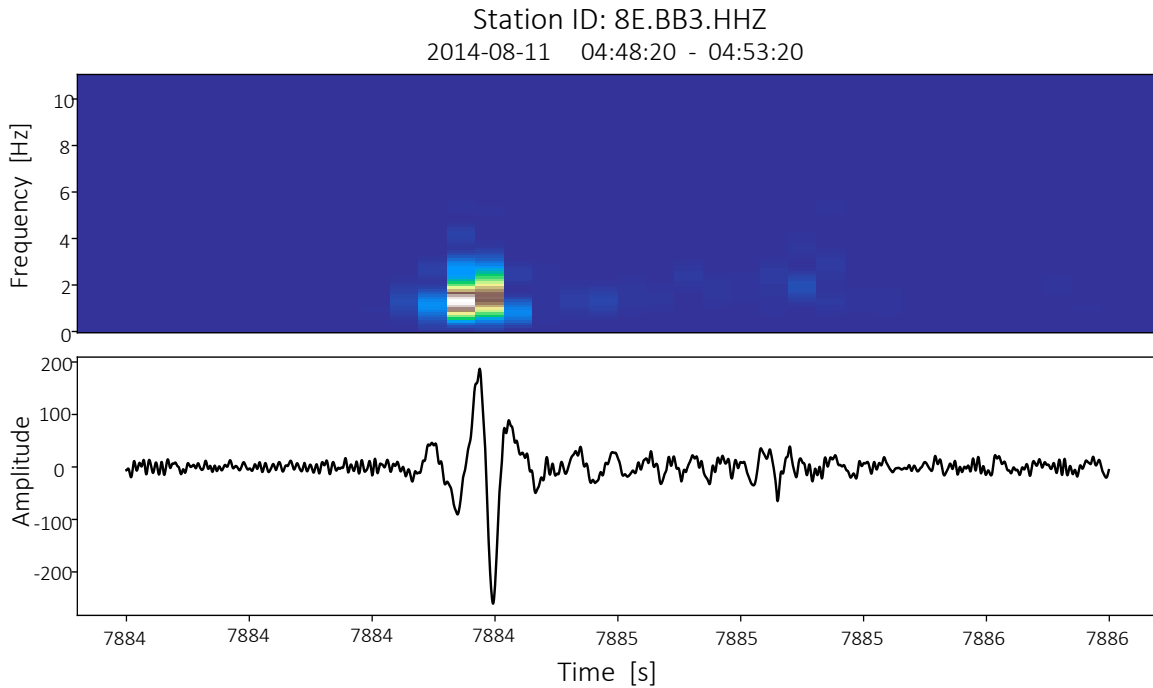


**Figure 17.** Very Long Frequency event recorded at Lascar volcano on BB5 station on June 30, 2014. a) Spectrogram for a VLF event, the frequency content ranges from 0.2 to 4 Hz. b) Seismogram for VLP occurred from 21:54:05 to 21:54:09.

#### 4.8 Event Location

Using the high frequency events identified in at least three stations, we will apply the grid method (Section 3.8.1) to find the approximate location of the event. We will locate the 2373 high frequency events. For reproducibility, the code for event location is included in Annex 4.

We generated a grid of 20000 x 22000 with a resolution of 5 meters, resulting in 440000000 grid points. We then calculated the distance between each station and every grid point. To determine the most appropriate velocity estimate ( $V_{\text{guess}}$ ), we tested different velocities ranging from 0.5 to 5 km/s. We selected ten random high-frequency events that had been recorded in at least four stations (Table 3) and used them to derive our  $V_{\text{guess}}$  estimate.

Multiple  $V_{\text{guess}}$  values were tested and their standard deviations were plotted against each other (Figure 18). The velocity value with the lowest standard deviation was selected as the most suitable velocity for each event. We obtained velocity values ranging from 3.5 to 4.8 km/s (Table 4). When comparing the events of July 7, 2014 (Figure 18a) and July 19, 2014

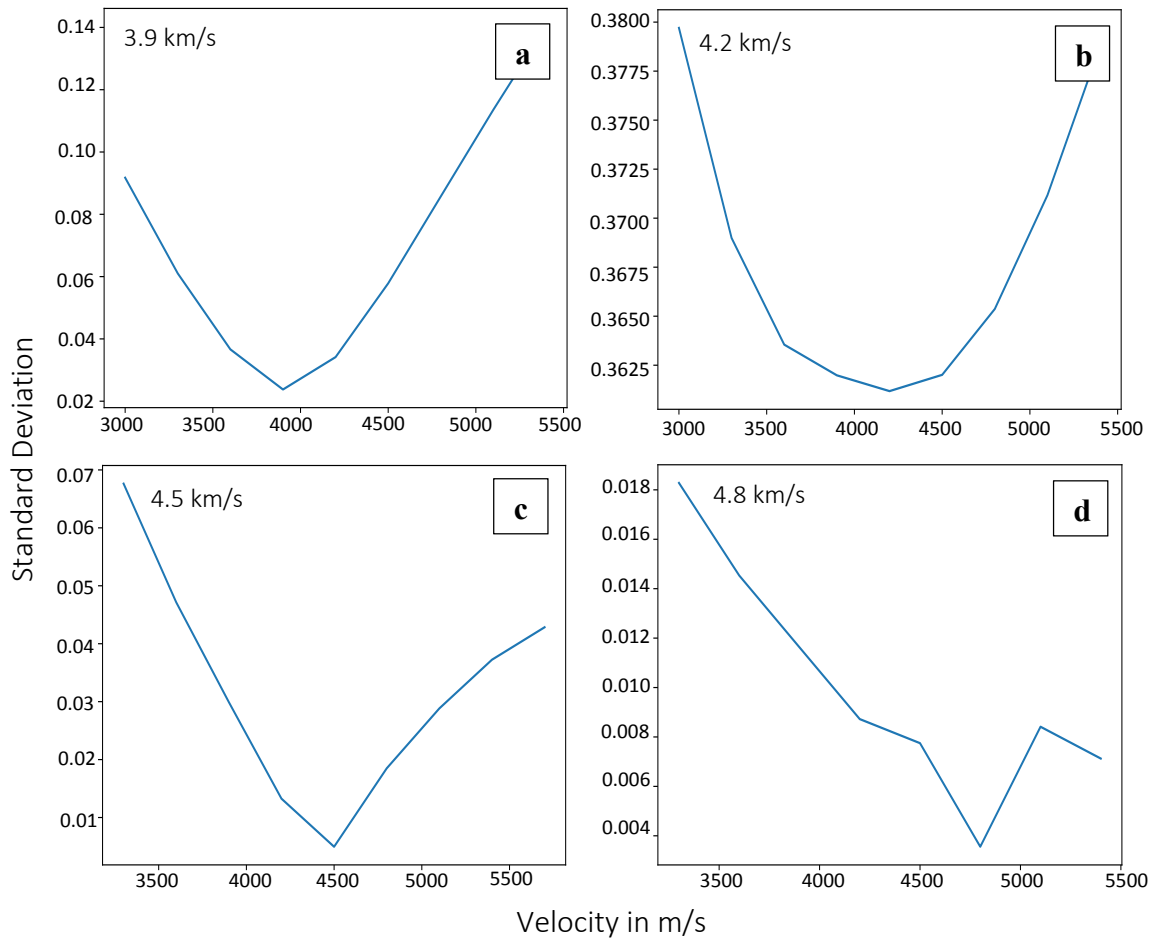


**Figure 18.** Velocity estimation for the location of four different high-frequency events. The best velocity, producing the minimum standard deviation, is listed for each event.

(Figure 18b), it can be observed that the lowest standard deviation in velocity occurs at a speed of 4 km/s. However, in contrast, the velocity change is more abrupt for the events on March 25, 2015 (Figure 18c) and May 20, 2015 (Figure 18d). This variation in velocity estimation shows the differences between events suggesting that the energy waves generated during each event may have encountered varying geological features or underwent different levels of attenuation, leading to distinct velocity patterns. Therefore, for subsequent calculations, we will use the average velocity of 4.46 km/s derived from the ten selected events (Figure 18). One of the selected event locations is shown in Annex 5.

After setting the velocity, we proceeded to determine the locations of high-frequency events. Figure 19 displays the resulting locations of high frequency events that were recorded

between 2014 and 2015. The majority of VT activity is concentrated in the southwestern part of the volcano, and a linear trend is noticeable towards the southwest with a significant change in slope close to the BB4 station. Some activity is also concentrated around the active crater. In 2014, there are fewer HF events, particularly around the active crater, which changes in the following year. In 2015, there is an increase in the number of HF events compared to the previous months. The spatial distribution remains similar between 2014 and 2015, but more events are observed around the crater, particularly in the southwestern part of the volcano's edifice. The events are primarily concentrated near the ancient Lascar edifice.

**Table 4.** Description of selected events for velocity estimation. Arrival time (Tarr) values are in seconds and Vguess values are in km/s

Date	Tarr	Station	Vguess	Date	Tarr	Station	Vguess
08/02/2015	2303.7	BB2	4.5	31/05/2014	22432.3	BB1	4.3
	2303.25	BB3			22432.0	BB3	
	2303.42	BB4			22432.6	BB4	
	2304.62	BB5			22432.2	BB5	
16/04/2015	2807.9	BB2	4.5	16/07/2014	22852.4	BB1	4.5
	2807.64	BB3			22851.8	BB3	
	2807.79	BB4			22851.9	BB4	
	2808.99	BB5			22852.9	BB5	
02/04/2015	2955.5	BB2	4.8	04/07/2014	25176.1	BB1	3.9
	2955.94	BB3			25175.3	BB3	
	2955.71	BB4			25175.1	BB4	
	2955.74	BB5			25176.5	BB5	
25/03/2015	9555.41	BB2	4.5	20/05/2015	3321.64	BB2	4.8
	9555.1	BB3			3321.25	BB3	
	9555.13	BB4			3322.35	BB4	
	9556.42	BB5			3321.01	BB5	
13/05/2014	15708.29	BB1	4.6	19/07/2014	68889.2	BB1	4.2
	15708.8	BB3			68887.7	BB3	
	15708.82	BB4			68887.8	BB4	
	15708.29	BB1			68888.8	BB5	

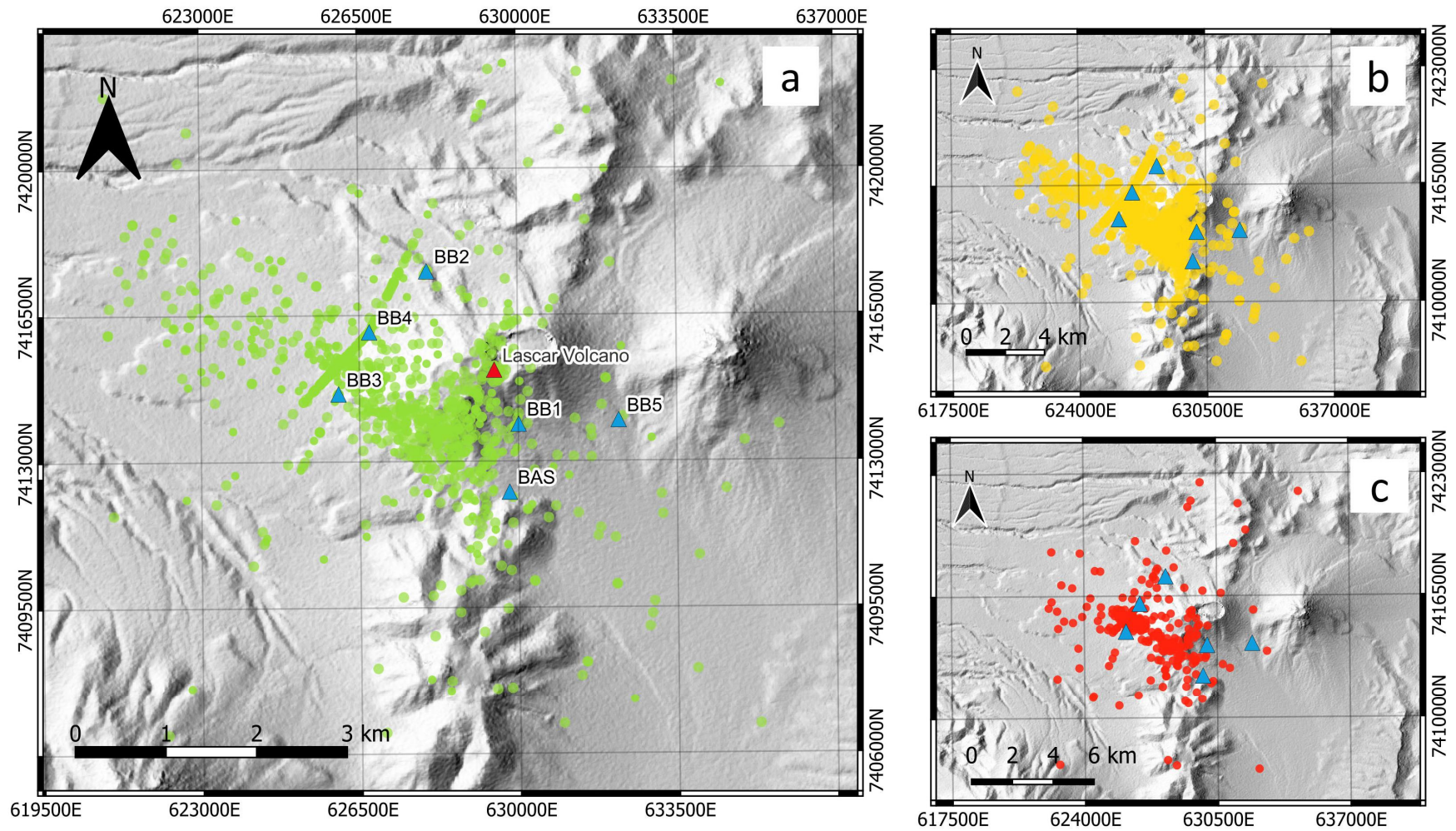


**Figure 19.** Location estimation for high frequency events recorded at Lascar volcano during 2014-2015. a) High frequency events recorded from January 2014 to May 2015 (green circles). b) High frequency events recorded in 2015 (yellow circles). c) High frequency located events in 2014 (red circles).

## 5 DISCUSSION

We have demonstrated that we can identify, classify, and locate seismic events using the five stations that recorded volcanic unrest at Lascar volcano from 2014 - 2015. We analyzed different aspects of the seismic signals by the metrics calculation, then we compare our results to those of previously published studies which used other methods, and discuss the benefits and limitations of our chosen methods. Finally, we discuss the observed events and what they might mean in terms of the volcanic activity at Lascar volcano

### 5.1 Temporal, amplitude and spectral metrics

We applied different metrics that analyze different aspects of the volcano-seismic signals. It is important to mention that not all the information is captured by the nine metrics. For that, it is crucial to consider the limitations associated with each metric. By doing this, we can make sure that the data is well understood and mitigate possible misinterpretations.

All these metrics applied to Lascar gave us valuable insights into the volcano dynamics. Most of the duration of the events is below the hundred seconds after the beginning of the event. This means that most of the Lascar activity is short-duration. On the other hand, we have recognized events that last up to three hours. These events suggest a gradual release of energy with some minor changes from December to May 2015 since we have identified six possible explosion quakes. We tried to identify some patterns or clusters of event occurrence, but it was not feasible since gap and event rate metrics are not enough to define clusters (Figure 21). The event rate does not show abrupt changes or significant increases in volcanic events. Even though we identified a positive trend from December 2014 to May 2015 (Figure 22), during this time, the gap started decreasing. There was identified about to 70 high- and low-frequency events recorded on January and April 2015; the maximum number of events recorded. The RMSa, phase amplitude and the maximum frequency were the metrics that reduced most of the noise. We identified some relationship between the frequency index and the maximum amplitude. The inverse relationship between the FI and the maximum amplitude is concordant with the RMS amplitude, the lower the FI the higher the strength of the signal according to the RMSa.

## 5.2 Comparison with published study

“Seismic activity during 2013-2015 intereruptive phase at Lasca volcano, Chile” published by Gaete and colleagues in 2019 analyze seismic signals at Lascar. The study aimed to understand the inner processes and deep structure of the volcano by analyzing seismic events and their locations. The authors used a seismic event catalog developed by the Observatorio Volcanológico de los Andes del Sur (OVDAS), the public institution responsible for monitoring Lascar. The OVDAS data network provided 2,893 classified local seismic events from January 1, 2013, to December 25, 2015, including 2,000 long-period events, 350 volcano-tectonic events, and 543 hybrid, explosion, and tremor events.

Our study, which used data from 2014 to 2015 (approximately seven months), identified a total of 2,951 seismic events across at least three monitoring stations. These events were categorized into 1,373 high-frequency events, 984 low-frequency events, 588 hybrid events, and 6 explosion events. However, it should be noted that the high-frequency event category may include other types of earthquakes in addition to VT events, and the same principle applies to the low-frequency event category.

The study by Gaete and colleagues focused on volcano-tectonic and long-period signals and their characteristics for location analysis. LP events were found to have frequency bands between 0.2 and 10 Hz, while VT events had frequencies above 5 Hz. This was also found in our study, most of the frequency spectra was concentrated between 0.2 to 20 Hz. In addition, we found that the majority of low frequency events were concentrated between 0.05 to 2 Hz, which is also in agreement with the published result in the LP location analysis section.

To determine the location of the VT events more accurately, the authors used the Hypo71 program to relocate them. The authors also used two velocity models (Comte et al., 1994, and Dorbath et al., 2008) to estimate a P-wave velocity of 4.39 km/s within a 5 km radius of Lascar. As part of our location analysis, we estimated the P-wave velocity at Lascar, resulting in an average velocity of 4.46 km/s, which was similar to the velocity estimate derived from the velocity models.



We located the high frequency events on the map provided by Gaete et al. and observed differences between our study and theirs. Our study area was larger than theirs, so we clipped the area to make a fair comparison (Figure 20). Most of our event locations are concentrated in the SW flank of the volcano, similar to Gaete et al.'s findings. However, these events are closer to the crater but in the same direction. The differences in event density can be related to the number of events; our catalogue is larger than theirs. Therefore, in a bigger picture, the orientations of the VT events are similar. However, we recommend further improvement in event noise removal by comparing the three-channel signal, not just the vertical component as we did.

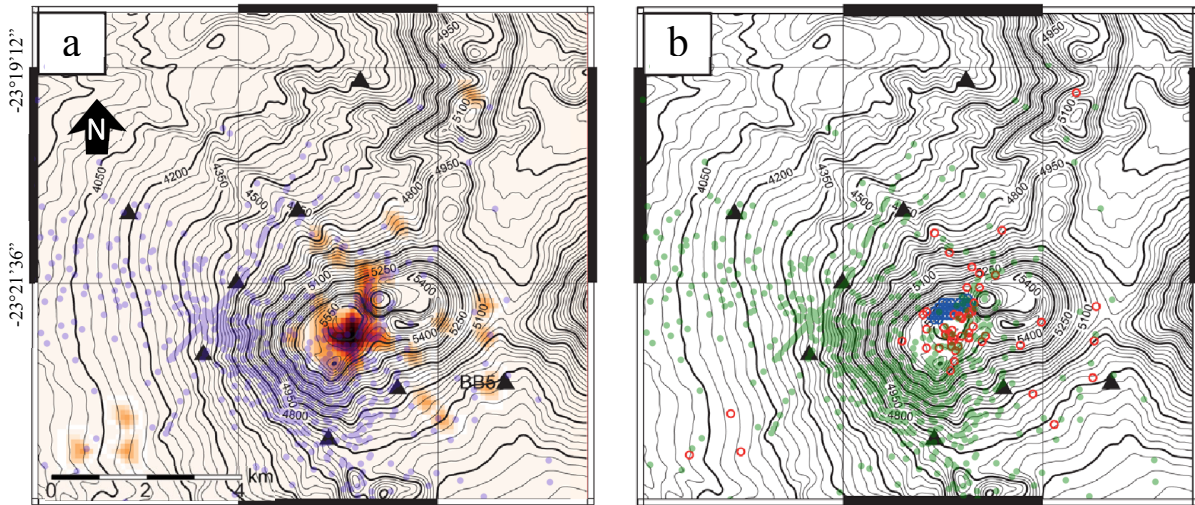


**Figure 20.** A comparison of volcano-tectonic earthquake (VT) locations. b) VT event locations found in our study (blue dots), and VT events found by Gaete et al. (2019; orange dots). c) locations of VTs (in green) from our study and the VTs (red circles) and long-period (LP) events (blue circles) published by Gaete et al. (2019).

### 5.3 Multistation vs Single Station Detection

There is a significant difference between the number of events obtained from the Multistation and SSD methods in this study. For station BAS, we identified 4543 events from January to April 2014 after noise removal, while for BB1, BB2, BB3, BB4, and BB5, we identified a total of 2951 events from May to August 2014 and from December 2014 to May 2015. Despite the smaller time period used for SSD, SSD identified more events than Multistation. This suggests that the thresholds for noise removal should be stricter to remove possible false

positive events. Additionally, new metrics based on amplitude, temporal, or spectral signal characteristics may be useful.

#### **5.4 Benefits and Limitations**

Our study has yielded a more comprehensive catalog of Lascar volcanic activity, surpassing the findings of previous studies and publications. This has provided us with a more robust understanding of the distribution of events and its implications. However, it's important to acknowledge that our approach has limitations. While we were able to classify events into four major clusters - high frequency, low frequency, hybrid, and explosive events - we couldn't differentiate between event types like VT a-type, VT b-type, volcanic shock, tremors, VLP, etc. Nevertheless, these larger clusters have been helpful in understanding the dynamics of the volcano in a simplified way.

To understand the geophysical characteristics of Lascar, we used a simple calculation to determine the location of high frequency events. Given the complexity of this volcanic environment, not all methods can be employed effectively. We employed a grid method using only one location-based parameter, arrival time. By comparing various values of velocities, we were able to find an approximate value that worked for most events. While this technique may not work for other volcanic environments, we found that our estimation was comparable to those obtained through other methods such as 2-D models and structural analysis (Comte et al., 1994), or double-difference tomography (TomoDD) using robust seismic networks (Dorbath et al., 2008).

#### **5.5 Interpretations of Events**

To gain a better understanding of the significance of seismic events, we calculated the daily average of long-period events. We also analyzed the ratio between LP and volcano-tectonic events. As we described earlier, LP and VT events are associated with different processes in a volcanic environment. An increase in the number of LP events may indicate movement of magma within the volcano, while an increase in VT signals can be associated with increasing stress in the volcanic system. Therefore, an increase in the LP/VT ratio may indicate an impending eruption. However, it is important to note that the LP/VT ratio alone is not sufficient to predict an eruption accurately. Other data, such as gas emissions, ground

deformation, and visual observations, must be considered to assess volcanic activity and forecast eruptions.

We calculated the daily average of long-period/volcano-tectonic events, as well as the daily LP average for stations BB1, BB2, BB3, BB4, and BB5, using all available data (Figure 21). It reveals several spurious peaks that are not consistent over time, such as the peak observed in April 2014. However, a consistent increase in the LP/VT ratio and LP average is observed between July 2014 and September 2014 (marked by a blue rectangle in Figure 21). This increase could mark the initial phase of Lascar unrest, which ultimately led to the October 2015 eruption. A gap in the data prevents us from understanding the evolution of the volcanic

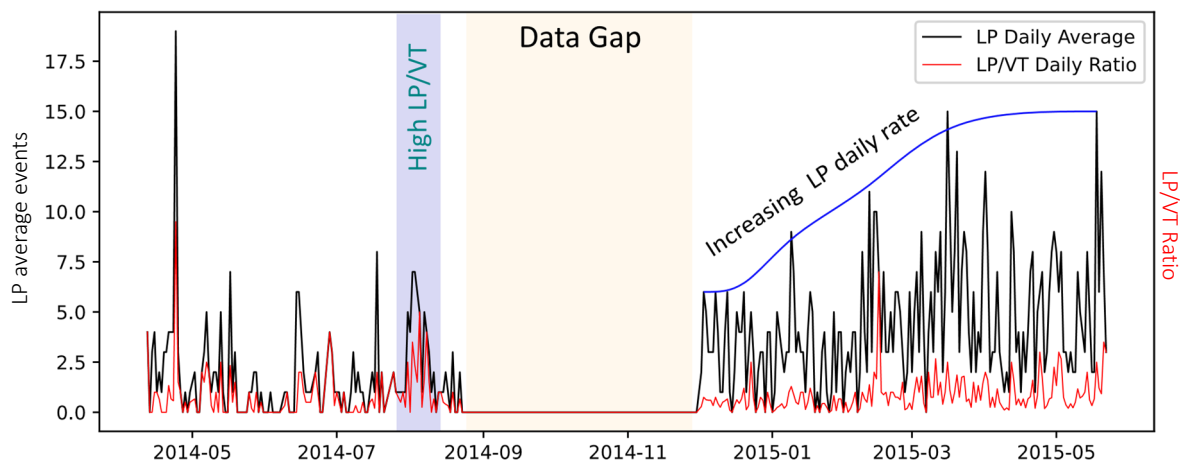


**Figure 21.** Daily average of Long-Period events and LP/VT ratio calculated from April 2014 to May 2015

system during this period. However, after this gap, the LP average continues to increase constantly until May 2015. This finding is in line with the trend observed in Figure 22, which shows a constant maximum value of event rate from January to July 2014, followed by an anomalous peak in August of the same year. Subsequently, after the data gap, the event rate continues to rise towards May 2015. Therefore, it is clear that volcanic activity at Lascar increased continuously, highlighting the importance of monitoring future changes in the volcanic system.

The concentration of volcano-tectonic events (Figure 19) in the southwest region of the volcanic edifice provided important insights into the volcanic dynamics. These events can

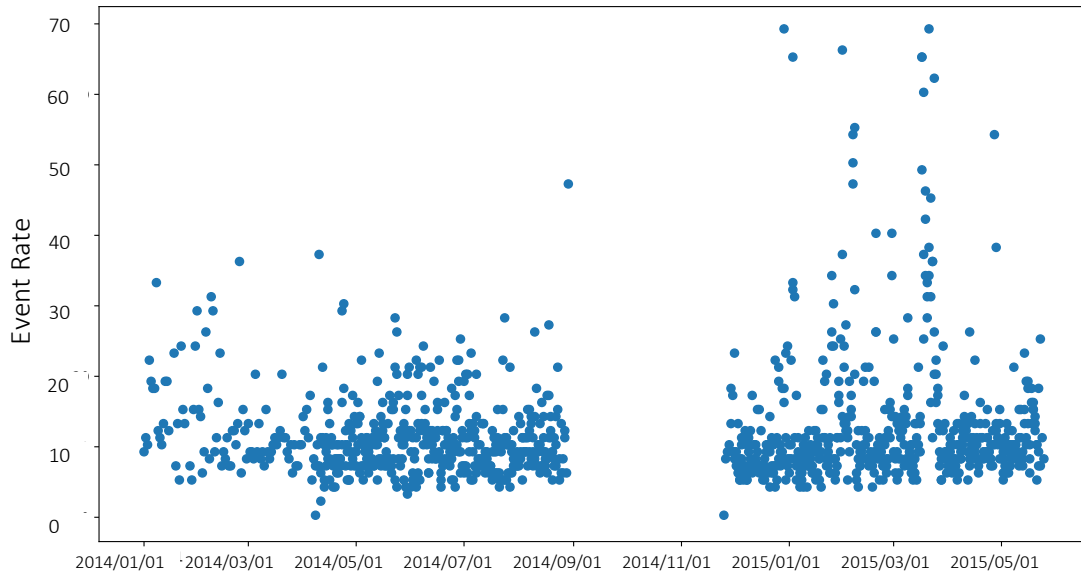


**Figure 22.** Event rate maximum value for each day in the period 1 January 2014 - 25 May 2015.

indicate stress and pressure changes within the volcano. The clustering of VT events in the southwest area may suggest a migration of the volcanic activity towards the older edifice. However, it is important to note that the interpretation of VT events alone is not sufficient to draw definitive conclusions about the behavior of the volcano.

To obtain more consistent interpretations, additional methods, such as geodetic and gas monitoring, should be employed to supplement the seismic data. By analyzing multiple types of data, scientists can better understand the complex processes that drive volcanic activity and make more accurate predictions about potential hazards.

## 6 CONCLUSIONS

In conclusion, our study has demonstrated the importance of seismic monitoring networks for characterizing volcanic activity at Lascar volcano, Chile. We have shown that seismic signals can provide valuable insights into the internal processes of the volcano, as well as the structure and dynamics of magmatic bodies and plumbing systems. Our methodology for identifying and characterizing volcanic events using seismic signals has allowed us to classify different types of seismic signals and volcanic events based on their properties and

mechanism. The STA/LTA ratio and metrics used in this study proved to be highly effective in recognizing and filtering seismic events recorded at Lascar volcano. We have also identified several LP, VT, and Hybrid events, as well as Explosive events. The results obtained demonstrate the applicability of this methodology in other volcanic environments and its ease of adaptation, especially in areas with challenging monitoring conditions or limited funds for installing and maintaining seismic stations.

Additionally, we locate the high frequency events and compare our results with previous studies. We analyze the time distribution using event rates. Our findings suggest that Lascar volcano experienced a prolonged period of seismic quiescence prior 2013, followed by an increase in seismic activity from 2014 to 2015, which may indicate the onset of a new eruptive cycle.

This study also provides insights into the seismicity and volcanic activity at Lascar Volcano. We observed a clustering of high-frequency events in the southwestern region of the volcano, indicating the presence of pressure or stress changes. Furthermore, the migration of magmatic activity towards the southwest flank of Lascar, as suggested by the location of some of the volcanic events, highlights the importance of continued monitoring efforts. Overall, our study highlights the importance of seismic monitoring of Lascar volcano and other volcanoes, as well as the need for ongoing research to improve our understanding of volcanic processes and hazards.

## **6.1 Recommendations and Future Work**

While there are numerous recommendations mentioned throughout this study, the following are the most critical:

1. Continuation of seismic monitoring: Given the importance of seismic signals for understanding volcanic activity, continued monitoring of Lascar's seismic activity is crucial. This could involve upgrading and expanding existing monitoring networks, as well as incorporating additional stations for deformation analysis, GPS or satellite imagery.
2. Integration of multiple data sources: To gain a more complete picture of volcanic activity at Lascar, future studies could integrate seismic data with other types of data

such as gas emissions, thermal imagery, and satellite data. This could help to identify patterns and correlations between different types of volcanic activity.

3. Improved understanding of magma storage and transport: To better understand the behavior of Lascar's magmatic system, future studies could focus on characterizing the location, size, and geometry of magma reservoirs beneath the volcano. This could involve geophysical surveys, geochemical analyses of volcanic rocks and fluids, and numerical modeling.

As mentioned previously, the methodology used in this study can be applied to complex volcanic systems and dynamics. Even though this study focused on Lascar volcano, the variables and parameters can be adjusted to make the methodology applicable to other highly active volcanoes, such as Reventador or Tungurahua in Ecuador. These two volcanoes have similar geological and seismic characteristics to Lascar. With the seismic data from at least two stations, we can establish appropriate thresholds to obtain high-quality seismic catalogs, and with seismic data from at least 3 stations, we can perform simple grid search location analyses for high frequency events. By analyzing and understanding the geological processes occurring deep beneath the volcano, we can improve our understanding of the volcanic system and potentially identify precursory signals of volcanic activity. Therefore, it is recommended to use this methodology to investigate other volcanoes in Ecuador and other regions with similar geological and seismic characteristics.

## 7 REFERENCES

- Allahverdiyeva, N. R. (2022, May). Preprocessing of Seismic Data using Neural Networks. In *2022 8th International Conference on Control, Decision and Information Technologies (CoDIT)* (Vol. 1, pp. 569-575). IEEE.
- Bertin, D., Lindsay, J., Cronin, S., Silva, S. de ., Connor, C., Caffè, P., Grosse, P., Báez, W., Bustos, E., & Constantinescu, R. (2022). Volcanic geospatial database of the Chilean-Argentinian segment (22.5-29°S) of the Central Volcanic Zone of the Andes (Version 4)[Data set]. The University of Auckland. <https://doi.org/10.17608/k6.auckland.16894903.v4>

- Beyreuther, M., Barsch, R., Krischer, L., Megies, T., Behr, Y., and Wassermann, J. (May/June 2010), ObsPy: A Python Toolbox for Seismology. *Seismological Research Letters*, 81 (3), 530-533. [http://www.seismosoc.org/publications/SRL/SRL\\_81/srl\\_81-3\\_es/](http://www.seismosoc.org/publications/SRL/SRL_81/srl_81-3_es/)
- Beyreuther, M., Barsch, R., Krischer, L., Megies, T., Behr, Y., and Wassermann, J. (May/June 2010), ObsPy: A Python Toolbox for Seismology, *Seismological Research Letters*, 81 (3), 530-533. [http://www.seismosoc.org/publications/SRL/SRL\\_81/srl\\_81-3\\_es/](http://www.seismosoc.org/publications/SRL/SRL_81/srl_81-3_es/)
- Bisztricsany, E. (1958). A new method for the determination of the magnitude of earthquakes. *Geofiz. Kozlemen*, 7(2).
- Body waves inside the earth. Earthquake.usgs.gov. (2021). Retrieved 4 November 2021, from <https://earthquake.usgs.gov/earthquakes/events/1906calif/18april/earthwaves.php>.
- Brenguier, F., Clarke, D., Aoki, Y., Shapiro, N. M., Campillo, M., & Ferrazzini, V. (2011). Monitoring volcanoes using seismic noise correlations. *Comptes Rendus Geoscience*, 343(8), 633–638. <https://doi.org/https://doi.org/10.1016/j.crte.2010.12.010>
- Brill, K. A., Waite, G. P., & Chigna, G. (2018). Foundations for forecasting: Defining baseline seismicity at fuego volcano, Guatemala. *Frontiers in Earth Science*, 6(July), 1–18. <https://doi.org/10.3389/feart.2018.00087>
- Buurman, H., West, M., 2010. Seismic precursors to volcanic explosions during the 2006 eruption of Augustine Volcano. In: Power, J., Coombs, M., Freymueller, J. (Eds.), *The 2006 eruption of Augustine Volcano. U.S. Geological Survey Professional Paper 1769*, Alaska (U.S. Geological Survey Professional Paper 1769).
- Casertano, L., & Barozzi, R. (1961, August). Informe sobre el sistema volcánico de Lascar. In *Anales de la Facultad de Ciencias Físicas y Matemáticas* (Vol. 18, No. 18, pp. ág-303).

- Chen, H. (2020). Estimating elastic properties and attenuation factor from different frequency components of observed seismic data. *Geophysical Journal International*, 220(2), 794-805.
- Chouet, B., Dawson, P., Ohminato, T., Martini, M., Saccorotti, G., Giudicepietro, F., De Luca, G., Milana, G., & Scarpa, R. (2003). Source mechanisms of explosions at Stromboli Volcano, Italy, determined from moment-tensor inversions of very-long-period data. *Journal of Geophysical Research: Solid Earth*, 108(B1), ESE-7.
- Comte, D., Roecker, S. W., & Suárez, G. (1994). Velocity structure in northern Chile: Evidence of subducted oceanic crust in the Nazca Plate. *Geophysical Journal International*, 117(3), 625-639.
- Council, N. R. (1994). *Mount Rainier: Active Cascade Volcano*. Washington, DC: The National Academies Press. <https://doi.org/10.17226/4546>
- Council, N. R. (2006). *Improved Seismic Monitoring - Improved Decision-Making: Assessing the Value of Reduced Uncertainty*. Washington, DC: The National Academies Press. <https://doi.org/10.17226/11327>
- De Silva, S.L. 1989. Altiplano-Puna volcanic complex of the central Andes. *Geology* 17: 1102-1106.
- Dorbath, C., Gerbault, M., Carlier, G., & Guiraud, M. (2008). Double seismic zone of the Nazca plate in northern Chile: High-resolution velocity structure, petrological implications, and thermomechanical modeling. *Geochemistry, Geophysics, Geosystems*, 9(7).
- Driedger, C., Neal, C. A., Knappenberger, T. H., Needham, D. H., Harper, R. B., & Steele, W. P. (2004). Hazard information management during the autumn 2004 reawakening of Mount St. Helens Volcano, Washington. *A Volcano Rekindled: The Renewed Eruption of Mount St. Helens, 2006*, 505–519.
- Ereditato, D., & Luongo, G. (1997). Explosion quakes at Stromboli (Italy). *Journal of Volcanology and Geothermal Research*, 79(3–4), 265–276. [https://doi.org/10.1016/S0377-0273\(97\)00033-4](https://doi.org/10.1016/S0377-0273(97)00033-4)



- Falsaperla, S., Caltabiano, T., Donatucci, A., Giammanco, S., Langer, H., Messina, A., Salerno, G., Sortino, F., Spampinato, S., & Ferlito, C. (2020). Integrated monitoring of soil gases, plume SO<sub>2</sub> and volcanic tremor to detect impulsive magma transfer at Mt. Etna volcano (Italy).
- Farrell, J., Husen, S., & Smith, R. B. (2009). Earthquake swarm and b-value characterization of the Yellowstone volcano-tectonic system. *Journal of Volcanology and Geothermal Research*, 188(1-3), 260-276.
- Gaete, A., Walter, T.R., Bredemeyer, S., Zimmer, M., Kujawa, C., Franco Marin, L., San Martín, J.P., & Bucarey Parra, C. (2020). Processes culminating in the 2015 phreatic explosion at Lascar volcano, Chile, evidenced by multiparametric data. *Natural Hazards and Earth System Sciences*, 20, 377-397.
- Galluzzo, D., Nardone, L., La Rocca, M., Esposito, A. M., Manzo, R., & Di Maio, R. (2020). Statistical moments of power spectrum: A fast tool for the classification of seismic events recorded on volcanoes. *Advances in Geosciences*, 52, 67-74.
- Gardeweg, M., Amigo, A., Matthews, S., Sparks, R.S.J., Clavero, J., (2011). Geología del volcán Láscar, Región de Antofagasta. *Servicio Nacional de Geología y Minería, Carta Geológica de Chile, Serie Geología Básica* 131, 40 p. Santiago.
- Gardeweg, M.C. (1991). La actividad eruptiva 1986-1990 del Volcán Láscar (II Región). In *Congreso Geológico de Chile*, No. 6, Actas 1: 477-480. Viña del Mar.
- Gardeweg, M.C.; Fuentealba, G.; Murillo, M.; Petit-Breuilh, M.E.; Espinoza, A.; Moreno, M.; Sparks, R.S.J.; Matthews, S.J. (1994a). Volcán Láscar: Geología y Evaluación del Riesgo Volcánico-Altiplano II Región. Servicio Nacional de Geología y Minería, Informe Registrado (Inédito), IR-94-03: 169 p.
- Gardeweg, M.C.; Sparks, R.S.J.; Matthews, S.J. (1998). Evolution of Láscar Volcano, Northern Chile. *Journal of the Geological Society of London* 155: 89-104.
- Godano, C., Tramelli, A., Mora, M., Taylor, W., & Petrillo, G. (2023). An analytic expression for the volcanic seismic swarms occurrence rate. A case study of some volcanoes in the world. *Earth and Space Science*, 10(2), e2022EA002534.

- González-Ferrán, O. et al. (1995). Volcanes de Chile. Instituto Geográfico Militar.
- Gottschämmer, E., & Surono, I. (2000). Locating tremor and shock sources recorded at Bromo Volcano. *Journal of volcanology and geothermal research*, 101(1-2), 199-209.
- Harlow, D. H., Power, J. A., Laguerta, E. P., Ambubuyog, G., White, R. A., & Hoblitt, R. P. (1996). Precursory seismicity and forecasting of the June 15, 1991, eruption of Mount Pinatubo. *Fire and Mud: Eruptions and Lahars of Mount Pinatubo, Philippines*, 223–247.
- Havskov, J., & Alguacil, G. (2015). *Instrumentation in earthquake seismology. Instrumentation in Earthquake Seismology*. <https://doi.org/10.1007/978-3-319-21314-9>
- Hill, D. P. (1977). A model for earthquake swarms. *Journal of Geophysical Research*, 82(8), 1347-1352.
- Isaks, B. 1988. Uplift of the Central Andean Plateau and bending of the Bolivian Orocline. *J. Geophys. Res.*, 93, 3211 – 3231.
- Kettner, D., & Power, J. (2013). Characterization of seismic events during the 2009 eruption of Redoubt Volcano, Alaska. *Journal of Volcanology and Geothermal Research*, 259, 45-62.
- Krischer, L., Megies, T., Barsch, R., Beyreuther, M., Lecocq, T., Caudron, C., and Wassermann, J. (2015), ObsPy: a bridge for seismology into the scientific Python ecosystem, *Computational Science & Discovery*, 8 (1), 014003. <http://stacks.iop.org/1749-4699/8/i=1/a=014003>
- Lemenkova, P. (2019). Geomorphological modelling and mapping of the Peru-Chile Trench by GMT. *Polish Cartographical Review*, 51(4), 181-194.
- Mah S (2003) Discrimination of Strombolian eruption types using very long period (VLP) seismic signals and video observations at Mount Erebus, Antarctica, *M.S. Independent Study*, New Mexico Institute of Mining and Technology

- Matsumoto, H., Zampolli, M., Haralabus, G., Stanley, J., Mattila, J., & Meral Özel, N. (2019). Interpretation of detections of volcanic activity at Ioto Island obtained from in situ seismometers and remote hydrophones of the International Monitoring System. *Scientific Reports*, 9(1), 1-11.
- Matthews, S. J., Jones, A. P., & Gardeweg, M. C. (1994). Lascar Volcano, Northern Chile; evidence for steady-state disequilibrium. *Journal of Petrology*, 35(2), 401-432.
- Matthews, S., Marquillas, R., Kemp, A., Grange, F., and Gardeweg, M. (1996). Active skarn formation beneath lascar volcano, northern chile: a petrographic and geochemical study of xenoliths in eruption products. *Journal of Metamorphic Geology*, 14(4):509–530.
- Matthews, S., Sparks, R., and Gardeweg, M. (1999). The piedras grandes–soncor eruptions, lascar volcano, chile; evolution of a zoned magma chamber in the central andean upper crust. *Journal of Petrology*, 40(12):1891–1919.
- Matthews, S.J.; Gardeweg, M.C.; Sparks, R.S.J. (1997). The 1984 to 1996 cyclic activity of Láscar Volcano, Northern Chile; cycles of dome growth, dome subsidence, degassing and explosive eruptions. *Bulletin of Volcanology* 59: 72-82.
- McLaskey, G. C., Thomas, A. M., Glaser, S. D., & Nadeau, R. M. (2012). Fault healing promotes high-frequency earthquakes in laboratory experiments and on natural faults. *Nature*, 491(7422), 101–104. <https://doi.org/10.1038/nature11512>
- McNutt, S. R. (1996). Seismic Monitoring and Eruption Forecasting of Volcanoes: A Review of the State-of-the-Art and Case Histories. *Monitoring and Mitigation of Volcano Hazards*, 99–146. [https://doi.org/10.1007/978-3-642-80087-0\\_3](https://doi.org/10.1007/978-3-642-80087-0_3)
- McNutt, S. R. (2000). Seismic Monitoring. In H. Sigurdsson, B. Houghton, S. R. McNutt, H. Rymer, & J. Stix (Eds.), *Encyclopedia of Volcanoes* (p. 1095/1119). Academic Press.
- McNutt, S. R. (2005). Volcanic seismology. *Annual Review of Earth and Planetary Sciences*, 33, 461–491. <https://doi.org/10.1146/annurev.earth.33.092203.122459>
- Megies, T., Beyreuther, M., Barsch, R., Krischer, L., and Wassermann, J. (2011), ObsPy - What can it do for data centers and observatories?, *Annals of Geophysics*, 54 (1). <http://www.annalsofgeophysics.eu/index.php/annals/article/view/4838>

- Mickus, K. (2021). Geophysical methods. In Mohamed, A. M. O., Paleologos, E., & Howari, F. (Eds.). *Pollution Assessment for Sustainable Practices in Applied Sciences and Engineering* (pp. 199-287). Butterworth-Heinemann. doi: <https://doi.org/10.1016/B978-0-12-809582-9.00005-0>
- Montes, L., Vargas, C., & Pérez, G. (2005). Modeling and removal of back-scattered noise from rough topography in land seismic data. *CT&F-Ciencia, Tecnología y Futuro*, 3(1), 69–76.
- Pamungkas, T. D., & Ridwana, R. (2021, March). Conceptual interpretation seismic 3D using RMS amplitude and dip-azimuth attribute analysis for identification structure and facies model in physical geographic. *In IOP Conference Series: Earth and Environmental Science* (Vol. 683, No. 1, p. 012055). IOP Publishing.
- Parmentier, E. M. (2015). Mantle Dynamics. In P. Kearey & F. J. Vine (Eds.), *Treatise on Geophysics* (2nd ed., Vol. 7, pp. 17-36). Elsevier.
- Pérez, G. P. (2020). Estudio de estructuras magmáticas bajo el volcán Láscar mediante datos de magnetotelúrica y geodesia [Master's thesis, Universidad de Chile].
- Pesicek, J. D., Wellik, J. J., Prejean, S. G., & Ogburn, S. E. (2018). Prevalence of seismic rate anomalies preceding volcanic eruptions in Alaska. *Frontiers in Earth Science*, 6, 100.
- Petit-Breuilh, M.E. (2004). La historia eruptiva de los volcanes hispanoamericanos (Siglos XVI al XX). Exmo Publications Service. Island Council of Lanzarote-House of the Volcanoes: 431 p. Spain.
- Philippi, R. A. and Petermann, A. (1856). Die sogennante Wüste Atacama. *Communications Department: Justus Pertes Geographical Institute*. p. 52
- Ramírez, C.F., Gardeweg, M., (1982). Hoja Toconao. Servicio Nacional de Geología y Minería, Carta Geológica de Chile, No. 54, 122 p. Santiago.
- Rubin, A. M., & Gillard, D. (1998). Dike induced seismicity: theoretical considerations. *J. geophys. Res*, 103(10), 017-10.

- Sassa, K. (1935). Volcanic Micro-Tremors and Eruption-Earthquakes: (Part I of the Geophysical Studies on the Volcano Aso). *Memoirs of the College of Science, Kyoto Imperial University. Series A*, 18(5), 255–293.
- Scheibner, E., Moore, G. W., Drummond, K. J., Dalziel, C. Q., Moritani, T., Teraoka, Y., ... & Craddock, C. (2013). *Tectonic map of the circum-Pacific region, Pacific basin sheet* (No. 52). US Geological Survey.
- Schmid, F., Karstens, J., & Nomikou, P. (2021, April). Identification and interpretation of seismic short-duration events inside the Kolumbo submarine volcano in the Southern Aegean. In *EGU General Assembly Conference Abstracts* (pp. EGU21-250).
- Seropian, G., Kennedy, B. M., Walter, T. R., Ichihara, M., & Jolly, A. D. (2021). A review framework of how earthquakes trigger volcanic eruptions. *Nature Communications*, 12(1), 1004.
- Servicio Nacional de Geología y Minería (2012). Reporte especial de actividad volcánica (REAV) N° 22. [https://rnvv.sernageomin.cl/rnvv/TI\\_Santiago\\_prod/reportes\\_LB/2012/\\_20120921040804524REAV\\_N22\\_Antofagasta\\_31012012.pdf](https://rnvv.sernageomin.cl/rnvv/TI_Santiago_prod/reportes_LB/2012/_20120921040804524REAV_N22_Antofagasta_31012012.pdf)
- Servicio Nacional de Geología y Minería (2013a). Reporte Especial Actividad Volcánica (REAV) N°38 región de Antofagasta volcán Láscar 03 de Abril de 2013 11:00 hora local. [https://rnvv.sernageomin.cl/rnvv/TI\\_Santiago\\_prod/reportes\\_LB/2013/\\_20130403123312737REAV\\_Antofagasta-N38-03042013.pdf](https://rnvv.sernageomin.cl/rnvv/TI_Santiago_prod/reportes_LB/2013/_20130403123312737REAV_Antofagasta-N38-03042013.pdf)
- Servicio Nacional de Geología y Minería (2013b). Reporte Especial de Actividad Volcánica No. 39 región de Antofagasta Marzo - Abril 2013. [https://rnvv.sernageomin.cl/rnvv/TI\\_Santiago\\_prod/reportes\\_LB/2013/\\_20130410030029305REAV\\_Antofagasta\\_2013\\_abril\\_10.pdf](https://rnvv.sernageomin.cl/rnvv/TI_Santiago_prod/reportes_LB/2013/_20130410030029305REAV_Antofagasta_2013_abril_10.pdf)
- Servicio Nacional de Geología y Minería (2013c). Reporte Especial de Actividad Volcánica (REAV) región de Antofagasta volcán Láscar 26 de julio, 2013 hora: 19:45 hora local. [https://rnvv.sernageomin.cl/rnvv/TI\\_Santiago\\_prod/reportes\\_LB/2013/\\_20130813125216638REAV\\_Antofagasta\\_2013\\_Julio\\_26.pdf](https://rnvv.sernageomin.cl/rnvv/TI_Santiago_prod/reportes_LB/2013/_20130813125216638REAV_Antofagasta_2013_Julio_26.pdf)

- Servicio Nacional de Geología y Minería (2015). Reporte Especial de Actividad Volcánica (REAV) región de Antofagasta año 2015 octubre 30, 09:45 HL. [https://rnvv.sernageomin.cl/rnvv/TI\\_Santiago\\_prod/reportes\\_LB/2015/\\_20151030100023908REAV\\_Antofagasta\\_30-10-2015\\_LC3A1scar20.pdf](https://rnvv.sernageomin.cl/rnvv/TI_Santiago_prod/reportes_LB/2015/_20151030100023908REAV_Antofagasta_30-10-2015_LC3A1scar20.pdf)
- Smithsonian Institution. Global Volcanism Program, American Geological Institute, Geological Survey (U.S.), and Environmental Systems Research Institute (Redlands, Calif.), (2003). *Global GIS : volcanoes of the world ; volcano basic data* [Data set]. American Geological Institute. Retrieved from: <https://geodata.lib.berkeley.edu/catalog/harvard-glb-volc>
- Song, Z., Tan, Y.J., & Roman, D.C. (2023). Deep Long-Period Earthquakes at Akutan Volcano From 2005 to 2017 Better Track Magma Influxes Compared to Volcano-Tectonic Earthquakes. *Geophysical Research Letters*, 50.
- The ObsPy Development Team. (2022). ObsPy 1.3.0 (1.3.0). Zenodo. <https://doi.org/10.5281/zenodo.6327346>
- Tilling, R. I. (2008). The critical role of volcano monitoring in risk reduction. *Advances in Geosciences*, 14(August 2007), 3–11. <https://doi.org/10.5194/adgeo-14-3-2008>
- U.S. Geological Survey. (n.d.). *Comprehensive monitoring provides timely warnings of volcano reawakening*. USGS Science for a Changing World. Retrieved June 21, 2021, from <https://www.usgs.gov/natural-hazards/volcano-hazards/monitoring>
- Walter, T.; Gaete, A.; Mikulla, S.; Kujawa, C.; Salzer, J.; Zimmer, M. (2014): *Seismic monitoring at Lascar volcano after 2014 Iquique earthquake*. GFZ Data Services. Other/Seismic Network. doi:10.14470/3R7569753098.
- Wassermann, J. (2012). Volcano seismology. In *New manual of seismological observatory practice 2 (NMSOP-2)* (pp. 1–77). Deutsches GeoForschungsZentrum GFZ.
- Wauthier, C., Roman, D.C., & Poland, M.P. (2013). Moderate-magnitude earthquakes induced by magma reservoir inflation at Kīlauea Volcano, Hawai‘i. *Geophysical Research Letters*, 40, 5366 - 5370.

- Williams, R. A., Perttu, A., & Taisne, B. (2020). Processing of volcano infrasound using film sound audio post-production techniques to improve signal detection via array processing. *Geoscience Letters*, 7(1), 1-13.
- Yukutake, Y., Abe, Y., Honda, R., & Sakai, S. (2021). Magma Reservoir and Magmatic Feeding System Beneath Hakone Volcano, Central Japan, Revealed by Highly Resolved Velocity Structure. *Journal of Geophysical Research: Solid Earth*, 126.
- Zobin, V. M. (2012). *Introduction to volcanic seismology* (Second, Vol. 6). Colima-México: Elsevier.
- Zobin, V.M. (2003). Origin of volcano-tectonic events. In V.M. Zobin (Ed.), *Introduction to volcanic seismology* (First, Vol. 6, pp. 31-45). Observatorio Vulcanológico, Colima, Mexico: University of Colima Press.
- Zollo, A., Lancieri, M., & Nielsen, S. (2006). Earthquake magnitude estimation from peak amplitudes of very early seismic signals on strong motion records. *Geophysical Research Letters*, 33(23).

## 8 ANNEXES

### ANNEX 1: Events Recognition

The following Python code is used to process all the identified and clean events that were found in the six stations. It compares the arrival times and sort it from lowest to highest Tarr values, then group them according the 1.5 second threshold, the date and different station.

```
#=====
==

# First we create two functions, one to recognize if there is more than
one mode and the frequency. Then, the second function is the one that
creates the groups of events based in three characteristics: Tarr, date
and station.

def modes(lst):
    freq_dict = {}
    for elem in lst:
        if elem in freq_dict:
            freq_dict[elem] += 1
        else:
            freq_dict[elem] = 1
    max_freq = max(freq_dict.values())
    if max_freq > 2:
        modes = [k for k, v in freq_dict.items() if v == max_freq]
    else:
        modes = None
    freq = max(freq_dict.values())
    return modes, freq

def group_events(sublists, threshold_time, lengroup):
    sorted_events = sorted(sublists, key=lambda x: x[0])
    event_groups = []
    current_group = [sorted_events[0]]
    threshold = sorted_events[0][0] + threshold_time
    for sublist in sorted_events[1:]:
```

Continue... (1/5)



```

    if (sublist[0] < threshold and
        sublist[1] not in [x[1] for x in current_group] and
        sublist[2] == current_group[0][2]):
        current_group.append(sublist)
    else:
        event_groups.append(current_group)
        current_group = [sublist]
        threshold = sublist[0] + threshold_time

filtered_groups = []
for group in event_groups:
    if len(group) >= lengroup:
        filtered_groups.append(group)
return filtered_groups

#=====
from timeit import default_timer as timer
from datetime import timedelta
start = timer()
import pandas as pd
file = 'All_stations_all_events.csv'
df = pd.read_csv(file)
df.fillna(0, inplace=True)
date = df.Date.dropna().values
T_arr = df.Arrival_Time.dropna().values
T_off = df.Trigger_off.dropna().values
type = df.Type.dropna().values
station = df.Station.dropna().values
gap = df.Gap.dropna().values
FI = df.Frequency_Index.dropna().values
pamp = df.Phase_Amplitude.dropna().values
length = df.Length.dropna().values
#=====

```

Continue... (2/5)

```

maxamp = df.Maximum_Amplitude.dropna().values
maxfreq = df.Maximum_Frequency.dropna().values
cenfreq = df.Center_Frequency.dropna().values
rms = df.RMS_Amplitude.dropna().values

#=====
events = []
for e in range(0, len(station)):
    events.append([T_arr[e], station[e], date[e], type[e], FI[e],
maxamp[e], pamp[e], rms[e], maxfreq[e], cenfreq[e], length[e],
gap[e], T_off[e]])
#=====

final = group_events(events, 1.5, 3) # group_events(list of events, the
time threshold, minimum number of events per group)

import numpy as np
Event_type = []
event_type=[]
for i in range(0, len(final)):
    ty = []
    Fi = []
    for j in range(0, len(final[i])):
        ty.append(final[i][j][3])
        Fi.append(final[i][j][4])
    mode_fi, freqs = modes(ty)
    if mode_fi == None or len(mode_fi)>1:
        mean_fi = np.mean(Fi)
        if mean_fi >= -0.768550:
            event_type.append('HF')
            t = 0
            while t < len(final[i]):
                Event_type.append('HF')
                t += 1
#=====

```

Continue... (3/5)

```

if mean_fi <= -0.911470 and mean_fi >= -2.196439:
    event_type.append('LF')
    t = 0
    while t < len(final[i]):
        Event_type.append('LF')
        t += 1
if mean_fi < -0.768550 and mean_fi > -0.911470:
    event_type.append('HYB')
    t = 0
    while t < len(final[i]):
        Event_type.append('HYB')
        t += 1
if mean_fi < -2.196439:
    event_type.append('EXP')
    t = 0
    while t < len(final[i]):
        Event_type.append('EXP')
        t += 1
else:
    if mode_fi[0] == 'HF':
        event_type.append('HF')
        t = 0
        while t < len(final[i]):
            Event_type.append('HF')
            t += 1
    if mode_fi[0] == 'LF':
        event_type.append('LF')
        t = 0
        while t < len(final[i]):
            Event_type.append('LF')
            t += 1

```

Continue... (4/5)

```

if mode_fi[0] == 'HYB':

    event_type.append('HYB')

    t = 0

    while t < len(final[i]):

        Event_type.append('HYB')

        t += 1

if mode_fi[0] == 'EXP':

    event_type.append('EXP')

    t = 0

    while t < len(final[i]):

        Event_type.append('EXP')

        t += 1

#=====
We separate the HF events that will be used for VT event location.
#=====

vt_event = []

vt_type = []

for t in range(len(event_type)):

    if event_type[t] == 'HF':

        vt_event.append(final[t])

        vt_type.append(event_type[t])

dfevt = pd.DataFrame(zip(*[vt_event]), columns=['Events'])

dftypevt = pd.DataFrame(zip(*[vt_type]), columns=['Event_Type'])

df = pd.concat([dfevt, dftypevt], axis=1)

df.to_csv(Final_vt_Events_allstations_1.5s.csv')

#=====

```

**ANNEX 2:** Single Station Detection noise removal for stations BB1, BB2, BB3, BB4, and BB5.

Here we detail the thresholds used to remove noisy signals and noisy events from our catalog, and the number of noisy signals and events removed for each station.

**Annex 2.1.** SSD noise removal for station BB1.

Metrics Criteria	Noisy signal	Removed Noisy Events	N° Events
RMSa < 10	52	52	10881
MF < 0.05 Hz	264	155	10726
MF > 17 Hz	76	76	10650
PA/RMSa > 25	47	42	10608
FI > 0.4412	9	9	10599
L < 2 seconds	10	1	10598
CF/PA > 120	7	0	10598

**Annex 2.2.** SSD noise removal for station BB2.

Metrics Criteria	Noisy signal	Removed Noisy Events	N° Events
RMSa < 10	34	34	18393
MF < 0.05 Hz	302	181	18212
MF > 17 Hz	20	20	18192
PA/RMSa > 25	35	33	18159
FI > 0.4412	20	20	18139
L < 2 seconds	1	0	18139
CF/PA > 120	3	0	18139

**Annex 2.3.** SSD noise removal for station BB3.

Metrics Criteria	Noisy signal	Removed Noisy Events	N° Events
RMSa < 10	196	196	25568
MF < 0.05 Hz	545	510	25058
MF > 17 Hz	117	116	24942
PA/RMSa > 25	130	121	24821
FI > 0.4412	12	11	24810
L < 2 seconds	14	1	24809
CF/PA > 120	16	0	24809

**Annex 2.4.** SSD noise removal for station BB4.

Metrics Criteria	Noisy signal	Removed Noisy Events	N° Events
RMSa < 10	635	635	31684
MF < 0.05 Hz	258	238	31446
MF > 17 Hz	14	14	31432
PA/RMSa > 25	70	63	31369
FI > 0.4412	46	45	31324
L < 2 seconds	64	2	31322
CF/PA > 120	128	12	31310

**Annex 2.5.** SSD noise removal for station BB5.

Metrics Criteria	Noisy signal	Removed Noisy Events	N° Events
RMSa < 10	239	239	30080
MF < 0.05 Hz	737	721	29359
MF > 17 Hz	131	130	29229
PA/RMSa > 25	93	76	29153
FI > 0.4412	15	15	29138
L < 2 seconds	56	2	29136
CF/PA > 120	57	0	29136

### ANNEX 3: Final events after noise removal

Here, we present a comprehensive overview of the total number of events detected through SSD methods, specifically highlighting the counts for high frequency, hybrid, low frequency, and explosion events.

#### Annex 3. 1. Description of the type of event for each station after the noise removal.

Station	High Frequency	Hybrid	Low Frequency	Explosion
BAS	3224	239	1080	0
BB1	5538	1888	3082	90
BB2	7093	3102	7758	186
BB3	17380	2283	4946	200
BB4	14695	7186	9100	329
BB5	21201	2626	5170	139

## ANNEX 4: Events Location

This python code was meant to calculate the location for high frequency, first we set the grid and the resolution, in this case 5 meters. Also set the station location to calculate the distance between all grid points to each station.

```
#=====
import numpy as np
import pandas as pd
import ast
from scipy.spatial.distance import cdist
import matplotlib.pyplot as plt

station_locs =
np.array([[629798.2, 7412258.9], [630006.7, 7413884.8], [627994.1, 7417545.5],
[626036.7, 7414616.9], [626724.1, 7416094.8], [632215.5, 7413976]])

x_min, x_max = 620000, 640000
y_min, y_max = 7405000, 7425000
res = 5

x_vals = np.arange(x_min, x_max + res, res)
y_vals = np.arange(y_min, y_max + res, res)
xx, yy = np.meshgrid(x_vals, y_vals)
grid_coords = np.c_[xx.ravel(), yy.ravel()]
distances = cdist(grid_coords, station_locs)
distances = distances.reshape(xx.shape + (station_locs.shape[0],))
mins = [] # coordinates for the minimum of the standard deviation
vguess = 4.46 * 1000

#=====
file = 'All_HF_toLocation_1.5s.csv'
df = pd.read_csv(file)
df.fillna(0, inplace=True)

    for i in tarr_ind:
```

Continue... (1/6)



```

        distances_to_station = distances[:, :, i]
        result = tarr[i] - (distances_to_station / vguess)
        results.append(result)

stds = np.std(results, axis=0)
min_std = np.min(stds)
min_std_loc = np.argmin(stds)
min_std_x, min_std_y = np.unravel_index(min_std_loc, stds.shape)
mins.append([xx[min_std_x, min_std_y], yy[min_std_x, min_std_y]])
elif station[k] == station_combination[3]:
    tarr = [np.nan, np.nan, tarr_list[k][0], tarr_list[k][1],
tarr_list[k][2], tarr_list[k][3] ]
    tarr_ind = [2, 3, 4, 5] # tarr_ind = [0,1,2,3,4,5]
    results = []
    for i in tarr_ind:
        distances_to_station = distances[:, :, i]
        result = tarr[i] - (distances_to_station / vguess)
        results.append(result)

stds = np.std(results, axis=0)
min_std = np.min(stds)
min_std_loc = np.argmin(stds)
min_std_x, min_std_y = np.unravel_index(min_std_loc, stds.shape)
mins.append([xx[min_std_x, min_std_y], yy[min_std_x, min_std_y]])
elif station[k] == station_combination[2]:
    tarr = [np.nan, tarr_list[k][0], np.nan, tarr_list[k][1],
tarr_list[k][2], tarr_list[k][3]]
    tarr_ind = [1, 3, 4, 5] # tarr_ind = [0,1,2,3,4,5]
    results = []
    for i in tarr_ind:
        distances_to_station = distances[:, :, i]
        result = tarr[i] - (distances_to_station / vguess)
        results.append(result)

stds = np.std(results, axis=0)

```

Continue... (3/6)

```

min_std = np.min(stds)
min_std_loc = np.argmin(stds)
min_std_x, min_std_y = np.unravel_index(min_std_loc, stds.shape)
mins.append([xx[min_std_x, min_std_y],yy[min_std_x, min_std_y]])
elif station[k] == station_combination[0]: #['BB2', 'BB3', 'BB4']
    tarr = [np.nan,np.nan,tarr_list[k][0],tarr_list[k][1],
tarr_list[k][2], np.nan]
    tarr_ind = [2, 3, 4] # tarr_ind = [0,1,2,3,4,5]
    results = []
    for i in tarr_ind:
        distances_to_station = distances[:, :, i]
        result = tarr[i] - (distances_to_station / vguess)
        results.append(result)
    stds = np.std(results, axis=0)
    min_std = np.min(stds)
    min_std_loc = np.argmin(stds)
    min_std_x, min_std_y = np.unravel_index(min_std_loc, stds.shape)
    mins.append([xx[min_std_x, min_std_y],yy[min_std_x, min_std_y]])
elif station[k] == station_combination[1]: #['BB3', 'BB4', 'BB5'],
    tarr = [np.nan,np.nan,np.nan,tarr_list[k][0], tarr_list[k][1],
tarr_list[k][2]]
    tarr_ind = [ 3, 4, 5] # tarr_ind = [0,1,2,3,4,5]
    results = []
    for i in tarr_ind:
        distances_to_station = distances[:, :, i]
        result = tarr[i] - (distances_to_station / vguess)
        results.append(result)
    stds = np.std(results, axis=0)
    min_std = np.min(stds)
    min_std_loc = np.argmin(stds)
    min_std_x, min_std_y = np.unravel_index(min_std_loc, stds.shape)
    mins.append([xx[min_std_x, min_std_y],yy[min_std_x, min_std_y]])

```

Continue... (4/6)

```

elif station[k] == station_combination[4]: #['BB2', 'BB4', 'BB5'],
    tarr = [np.nan,np.nan,tarr_list[k][0],np.nan, tarr_list[k][1],
tarr_list[k][2]]
    tarr_ind = [2, 4, 5] # tarr_ind = [0,1,2,3,4,5]
    results = []
    for i in tarr_ind:
        distances_to_station = distances[:, :, i]
        result = tarr[i] - (distances_to_station / vguess)
        results.append(result)
    stds = np.std(results, axis=0)
    min_std = np.min(stds)
    min_std_loc = np.argmin(stds)
    min_std_x, min_std_y = np.unravel_index(min_std_loc, stds.shape)
    mins.append([xx[min_std_x, min_std_y],yy[min_std_x, min_std_y]])
elif station[k] == station_combination[6]: #['BB1', 'BB4', 'BB5'],
    tarr = [np.nan,tarr_list[k][0],np.nan,np.nan, tarr_list[k][1],
tarr_list[k][2]]
    tarr_ind = [1, 4, 5] # tarr_ind = [0,1,2,3,4,5]
    results = []
    for i in tarr_ind:
        distances_to_station = distances[:, :, i]
        result = tarr[i] - (distances_to_station / vguess)
        results.append(result)
    stds = np.std(results, axis=0)
    min_std = np.min(stds)
    min_std_loc = np.argmin(stds)
    min_std_x, min_std_y = np.unravel_index(min_std_loc, stds.shape)
    mins.append([xx[min_std_x, min_std_y],yy[min_std_x, min_std_y]])

```

Continue... (5/6)

```

elif station[k] == station_combination[7]: #['BB2', 'BB3', 'BB5'],
    tarr = [np.nan, np.nan, tarr_list[k][0], tarr_list[k][1], np.nan, tarr_list[k][2]]
    tarr_ind = [2, 3, 5] # tarr_ind = [0,1,2,3,4,5]
    results = []
    for i in tarr_ind:
        distances_to_station = distances[:, :, i]
        result = tarr[i] - (distances_to_station / vguess)
        results.append(result)
    stds = np.std(results, axis=0)
    min_std = np.min(stds)
    min_std_loc = np.argmin(stds)
    min_std_x, min_std_y = np.unravel_index(min_std_loc, stds.shape)
    mins.append([xx[min_std_x, min_std_y], yy[min_std_x, min_std_y]])
else: #['BB1', 'BB3', 'BB5']
    tarr = [np.nan, tarr_list[k][0], np.nan, tarr_list[k][1], np.nan, tarr_list[k][2]]
    tarr_ind = [1, 3, 5] # tarr_ind = [0,1,2,3,4,5]
    results = []
    for i in tarr_ind:
        distances_to_station = distances[:, :, i]
        result = tarr[i] - (distances_to_station / vguess)
        results.append(result)
    stds = np.std(results, axis=0)
    min_std = np.min(stds)
    min_std_loc = np.argmin(stds)
    min_std_x, min_std_y = np.unravel_index(min_std_loc, stds.shape)
    mins.append([xx[min_std_x, min_std_y], yy[min_std_x, min_std_y]])

df = pd.DataFrame(zip(*mins), columns=['Event_Location'])

df.to_csv('C:/Users/HP/Desktop/Thesis
Project/RESULTS/VT_events/HF_Location_5m_1.5s_versionlast.csv')

```

(6/6)

### ANNEX 5: Example for one high frequency event location

This is an example of VT event location, where the lower values of the standard deviation are represented in dark blue and higher values in lighter colors (Annex 5.1). The location of the active and the nested craters are highlighted (red triangle and blue circles) as well as the location of the stations (black circles). The minimum of the standard deviation represents the location of the event (white cross).

